Mast Cells Play a Key Role in Host Defense against Herpes Simplex Virus Infection through TNF-α and IL-6 Production

Rui Aoki[1], Tatsuyoshi Kawamura[1], Fumi Goshima[2], Youichi Ogawa[1], Susumu Nakae[3], Atsuhito Nakao[4], Kohji Moriishi[5], Yukihiro Nishiyama[2] and Shinji Shimada[1]

The essential contribution of mast cells (MCs) to bacterial host defense has been well established; however, little is known about their role in viral infections *in vivo*. Here, we found that intradermal injection with herpes simplex virus 2 (HSV-2) into MC-deficient $Kit^{W/Wv}$ mice led to increased clinical severity and mortality with elevated virus titers in HSV-infected skins. *Ex vivo* HSV-specific tetramer staining assay demonstrated that MC deficiency did not affect the frequency of HSV-specific cytotoxic T lymphocytes (CTLs) in draining lymph nodes. Moreover, the high mortality in $Kit^{W/W\text{-}v}$ mice was completely reversed by intradermal reconstitution with bone marrow–derived MCs (BMMCs) from wild-type, but not $TNF^{-/-}$ or $IL\text{-}6^{-/-}$ mice, indicating that MCs or, more specifically, MC-derived tumor necrosis factor (TNF) and IL-6 can protect mice from HSV-induced mortality. However, HSV did not directly induce TNF-α or IL-6 production by BMMCs; supernatants from HSV-infected keratinocytes induced the production of these cytokines by BMMCs without degranulation. Furthermore, IL-33 expression was induced in HSV-infected keratinocytes, and blocking the IL-33 receptor T1/ST2 on BMMCs significantly reduced TNF-α and IL-6 production by BMMCs. These results indicate the involvement of MCs in host defense at HSV-infected sites through TNF-α and IL-6 production, which is induced by keratinocyte-derived IL-33.

Journal of Investigative Dermatology (2013) **133,** 2170–2179; doi:10.1038/jid.2013.150; published online 9 May 2013

INTRODUCTION

Mast cells (MCs) are not only effector cells in allergic responses but are also initiator and regulator cells in both innate and adaptive immune responses (Galli *et al.*, 2005). They are widely distributed throughout the body, in particular at host/environmental interfaces such as the skin and airways, where they preferentially localize around nerves and blood vessels (Galli *et al.*, 2005). They can therefore act as important sentinels for the immune system and control effective innate responses against invading pathogens by releasing various mediators, including a diverse array of cytokines, chemokines, and lipid mediators (Metz and Maurer, 2007; Abraham and St John, 2010).

The development of MC-deficient mouse models allows testing of MC contribution to biological responses of interest, both through the analysis of experimental outcomes in MC-deficient mice and those in mice in which MC deficiency has been selectively repaired by local engraftment (Galli *et al.*, 2005; Metz and Maurer, 2007). Using this so-called "MC knock-in mouse" model, several studies have demonstrated that MCs are critical effector cells in eliciting protective immune responses against bacteria, and that MC-derived tumor necrosis factor-α (TNF-α) is largely responsible for bacterial clearance by inducing neutrophil recruitment into sites of infection (Echtenacher *et al.*, 1996; Malaviya *et al.*, 1996). For the many MCs located proximal to blood vessels, the release of factors such as other cytokines, histamine, proteases, and chemokines also contributes to increased local vascular permeability and recruitment of other participants in the inflammatory response at the site of infection (Abraham and St John, 2010).

In contrast to the well-established contributions of MCs to host defense against bacteria, the function of MCs in antiviral immunity has not been well defined. We and others have previously reported that Toll-like receptor 3 (TLR3)-, TLR7-, and TLR9-mediated activation of MCs can induce selective production of cytokines and chemokines, suggesting that MCs

[1]*Department of Dermatology, Faculty of Medicine, University of Yamanashi, Chuo, Yamanashi, Japan;* [2]*Department of Virology, Nagoya University Graduate School of Medicine, Nagoya, Japan;* [3]*Laboratory of Systems Biology, Center for Experimental Medicine and Systems Biology, Institute of Medical Science, University of Tokyo, Tokyo, Japan;* [4]*Department of Immunology, Faculty of Medicine, University of Yamanashi, Chuo, Yamanashi, Japan and* [5]*Department of Microbiology, Faculty of Medicine, University of Yamanashi, Chuo, Yamanashi, Japan*

Correspondence: Tatsuyoshi Kawamura, Department of Dermatology, Faculty of Medicine, University of Yamanashi, 1110 Shimokato, Chuo, Yamanashi 409-3898, Japan. E-mail: tkawa@yamanashi.ac.jp

Abbreviations: BMMC, bone marrow–derived mast cell; CTL, cytotoxic T lymphocyte; DC, dendritic cell; DLN, draining lymph node; HSV-2, herpes simplex virus-2; MC, mast cell; MOI, multiplicity of infection; NK, natural killer; TNF-α, tumor necrosis factor-α; TLR, Toll-like receptor; WT, wild type

Received 8 November 2012; revised 19 February 2013; accepted 5 March 2013; accepted article preview online 25 March 2013; published online 9 May 2013

are capable of secreting these mediators in response to virus-derived pathogen-associated molecular patterns (Kulka *et al.*, 2004; Matsushima *et al.*, 2004). Indeed, several viruses, including dengue virus and adenovirus, have been shown to activate MCs *in vitro* through TLR3, TLR7, and possibly other mechanisms (Dawicki and Marshall, 2007). Nevertheless, the *in vivo* contribution of MCs to host defense in viral infections is less clear, mainly because suitable mouse models of viral infection have not been tested in the "MC knock-in mouse" model until recently (Metz *et al.*, 2008; Abraham and St John, 2010). However, two very recent studies have revealed the *in vivo* role of MCs in protective immune responses against viral infection using "MC knock-in mouse" model, and demonstrated that natural killer (NK) and NK T-cell recruitment promoted by MCs or MC-derived antimicrobial peptides has a pivotal role in viral clearance during dengue virus or vaccina virus infection, respectively (St John *et al.*, 2011; Wang *et al.*, 2012).

Herpes simplex virus type 2 (HSV-2) is a sexually transmitted pathogen that infects more than 500 million people worldwide and causes most cases of genital herpes (Looker *et al.*, 2008). In cutaneous herpes simplex lesions of humans and in murine models, keratinocytes, dendritic cells (DCs), and infiltrating lymphocytes, especially HSV-specific CD8 T lymphocytes, are known to have a central role in controlling primary and recurrent HSV infections (Simmons and Tscharke, 1992; Chew *et al.*, 2009). Moreover, the important role of other innate immune effectors such as NK cells, NK T cells, plasmacytoid DCs, macrophages, and γδ T lymphocytes has been recently re-emphasized, either in direct immune control or via modulation of adaptive immune responses in HSV infection (Cheng *et al.*, 2000; Chew *et al.*, 2009; Melchjorsen *et al.*, 2009). However, very little *in vitro* and *in vivo* data exist regarding the role of MCs in HSV infections.

Here, we examined the *in vivo* contribution of MCs to the immune responses against HSV using the "MC knock-in mouse" model and demonstrated that MCs were critically involved in host defense at HSV-infected sites through TNF-α and IL-6 production. Our study also suggests an important role for IL-33 derived from HSV-infected keratinocytes as a trigger for the production of these inflammatory cytokines by MCs.

RESULTS

MC-deficient mice exhibit high mortality and local inflammation following cutaneous HSV infection

We first assessed the role of MCs *in vivo* by using a murine model of lethal HSV encephalitis (Corey and Spear, 1986), whereby peripheral infection with HSV involves local replication in the skin, followed by rapid dissemination of the virus via sensory axons, causing zosteriform lesions to spread from the primary inoculation site along the affected dermatomes, and leading to paralysis and death. Using this model, MC-deficient $Kit^{W/W\text{-}v}$ mice and $Kit^{+/+}$ wild-type (WT) mice were injected intradermally with HSV-2 (7.5×10^4 PFU) and were monitored for survival and scored for paralysis and skin lesions. Intriguingly, $Kit^{W/W\text{-}v}$ mice exhibited markedly decreased percent survival when compared with $Kit^{+/+}$ mice (Figure 1a). We also compared clinical severity in these mice by using the experimental autoimmune encephalomyelitis score, which reflects paralysis. The clinical score in $Kit^{W/W\text{-}v}$ mice was significantly higher than that in $Kit^{+/+}$ mice (Figure 1b). We obtained similar findings when we repeated the experiments with MC-deficient $Kit^{W\text{-}sh/W\text{-}sh}$ mice injected intradermally with HSV-2 (Supplementary Figure S1a and b online). As shown in Figure 1c, the zosteriform eruption in the skin lesions of $Kit^{W/W\text{-}v}$ mice appeared at an earlier time point, and exacerbated more rapidly and severely than that of $Kit^{+/+}$ mice. Consistent with these findings, histological examination of the zosteriform lesion in $Kit^{W/W\text{-}v}$ mice revealed increased inflammation and an extended infection area, as demonstrated by HSV glycoprotein D antigen expression in subepithelial tissue, when compared with that in $Kit^{+/+}$ mice, at 3 and 5 days post infection (Figure 1d and e). On the basis of this histopathological observation, we assessed whether MCs contribute to HSV clearance by measuring virus titers in the HSV-infected skins of $Kit^{+/+}$ and $Kit^{W/W\text{-}v}$ mice. The virus titers in $Kit^{W/W\text{-}v}$ mice rapidly increased, reaching maximal levels at day 5, and dropped afterward (Figure 1f). In contrast, the skin lesions of $Kit^{+/+}$ mice contained lower virus titers, which were sustained until day 7. These results suggested that the severe inflammation and mortality observed in $Kit^{W/W\text{-}v}$ mice may be attributed to impaired virus clearance during these early stages of HSV infection, particularly during the first 3 days.

MCs produce TNF-α and IL-6, but not IFN-α, in response to soluble factors released from HSV-infected keratinocytes

The impaired clearance of HSV-2 in the skin lesion of $Kit^{W/W\text{-}v}$ mice was observed during the first 72 hours after infection (Figure 1f), suggesting that MCs are involved in innate immunity, rather than acquired immunity, against HSV-2. In early immune responses in HSV infection, several studies highlight the importance of TNF-α for protection against lethal HSV encephalitis (Rossol-Voth *et al.*, 1991; Lundberg *et al.*, 2007). In addition, TNF-α has been shown to control HSV replication, independent of T and B cells (Feduchi *et al.*, 1989; Heise and Virgin, 1995). Other studies indicated that IL-6 and IFN-α decrease the susceptibility to HSV infection (Murphy *et al.*, 2008; Melchjorsen *et al.*, 2009). Consistent with these findings, we could detect the production of TNF-α, IL-6, and IFN-α at HSV-2 injection sites 72 hours after infection in WT mice (Supplementary Figure S3a online). Therefore, we next assessed whether HSV-2 directly induced cytokine production by BMMCs. However, MCs are resistant to HSV-2 infection (Supplementary Figure S4a online), and HSV-2 exposure did not induce TNF-α and IL-6 production or degranulation by BMMCs (Supplementary Figure S4b–d online).

Because the major cellular targets for HSV-2 were found to be epidermal keratinocytes in the skin lesion of $Kit^{+/+}$ and $Kit^{W/W\text{-}v}$ mice at 3 days after infection Figure 1d), we hypothesized that soluble factors released from HSV-infected keratinocytes may induce the cytokine production by MCs. Strikingly, as shown in Figure 2a and b, the supernatants of HSV-treated keratinocytes, Pam-212, induced significant TNF-α and IL-6 production by BMMCs in a multiplicity of infection (MOI)–dependent manner, whereas they failed to induce

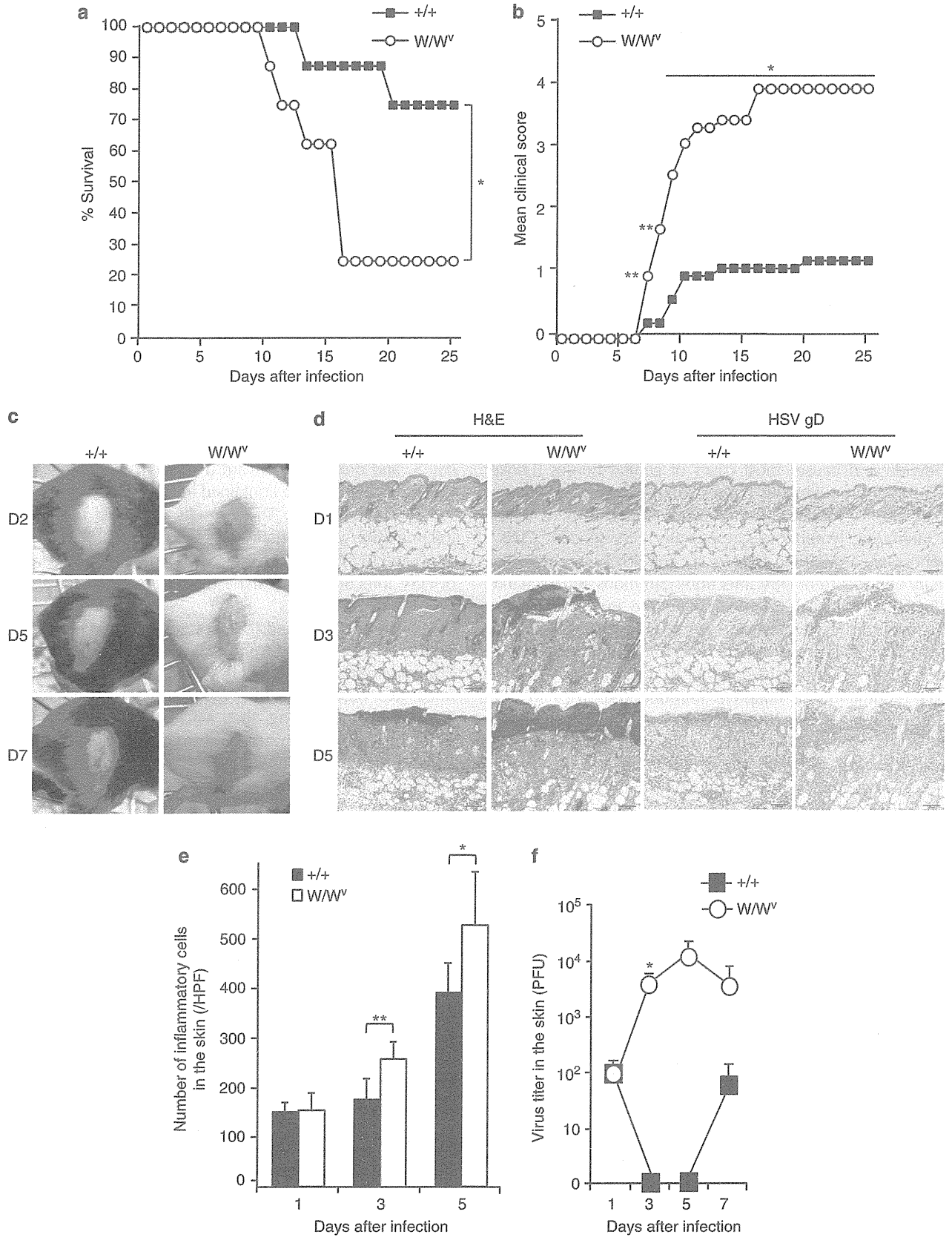
a
+/+
W/W^v
% Survival
Days after infection
b
Mean clinical score
Days after infection
c
+/+
W/W^v
D2
D5
D7
d
H&E
HSV gD
D1
D3
D5
e
Number of inflammatory cells in the skin (/HPF)
Days after infection
f
Virus titer in the skin (PFU)
Days after infection

degranulation in, and IFN-α production by, BMMCs (Figure 2c and d). Notably, *in vitro* HSV infection of keratinocytes did not directly induce the production of these cytokines (Supplementary Figure S3b online). These results imply that MCs may be capable of producing TNF-α and IL-6 in response to cutaneous HSV-2 infection *in vivo* by indirect stimulation via soluble factors derived from HSV-infected keratinocytes. Interestingly, as shown in Supplementary Figure S2a and c online, HSV-2 did not significantly increase MC degranulation in the skin *in vivo*.

MCs, particularly MC-derived TNF-α and IL-6, protect mice from HSV-induced severe mortality

To confirm whether the different responses against cutaneous HSV-2 infection in $Kit^{+/+}$ and $Kit^{W/W\text{-}v}$ mice observed in Figure 1 reflect the lack of MCs in $Kit^{W/W\text{-}v}$ mice rather than other c-Kit-related differences (Galli *et al.*, 2005), we examined $Kit^{W/W\text{-}v}$ mice locally reconstituted with BMMCs derived from $Kit^{+/+}$ mice (WT BMMC→$Kit^{W/W\text{-}v}$). As expected, the decreased survival rate and the severe clinical and lesion score in HSV-infected $Kit^{W/W\text{-}v}$ mice were significantly improved by local reconstitution with MCs, comparable to those in $Kit^{+/+}$ mice (Figure 3a–c). Nevertheless, local reconstitution of $Kit^{W/W\text{-}v}$ mice with BMMCs derived from TNF-deficient mice ($TNF^{-/-}$ BMMC→$Kit^{W/W\text{-}v}$) or IL-6-deficient mice ($IL\text{-}6^{-/-}$ BMMC→$Kit^{W/W\text{-}v}$) did not significantly improve percent survival, clinical score, or lesion score (Figure 3a–c). These results clearly indicate that both MC-produced TNF and IL-6 critically contribute to protective antiviral responses to HSV-2 *in vivo*.

IL-33 derived from HSV-2-treated keratinocytes can induce cytokine production by MCs

Next, we explored which soluble factors released by HSV-2-treated keratinocytes induce TNF-α and IL-6 production by MCs. Recent studies have highlighted the important roles of IL-33 as an "alarmin" in innate immune responses, as IL-33, as a key product of epithelial barrier tissues such as the skin, can be released into the extracellular space after epithelial cell damage during infection or trauma, and it functions as an alarmin to alert the immune system (Moussion *et al.*, 2008; Luthi *et al.*, 2009). It is notable that IL-33 has recently been shown to be upregulated in the lung during viral infection with influenza virus and spleen during infection with lymphocytic choriomeningitis virus (Chang *et al.*, 2011; Bonilla *et al.*, 2012). In line with these findings, we found that increased IL-33 expression was selectively detected on damaged or degenerating Pam-212 cells after *in vitro* HSV-2 exposure, and the frequency of IL-33-expressing cells was increased in an MOI-dependent manner (Figure 4a). In addition, we found a significant increase in IL-33 production by HSV-infected Pam-212 cells (Figure 4a). Importantly, we found that IL-6 and TNF-α production by BMMCs in response to the supernatants from HSV-2-treated Pam-212 cells was significantly and most effectively reduced by blockade of the IL-33 receptor using the T1/ST2 antibody (Figure 4b). Conversely, IL-6 production was not affected by neutralization of other cytokines including IL-1α, IFN-β, and thymic stromal lymphopoietin (Supplementary Figure S5 online). Furthermore, we found that IL-33 stimulates the production of TNF-α and IL-6 by BMMCs in a dose-dependent manner (Figure 4c), without inducing degranulation (data not shown). On the basis of these results,

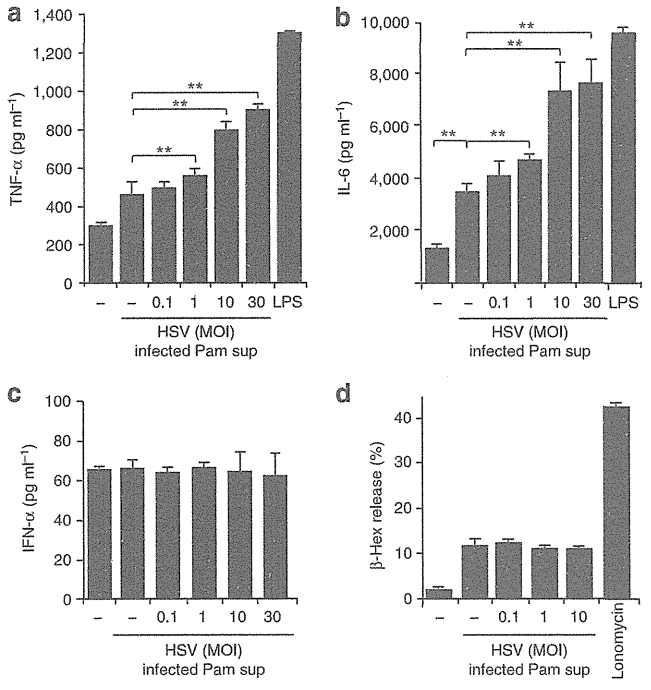

Figure 2. Supernatants of herpes simplex virus 2 (HSV)–infected keratinocytes induce tumor necrosis factor-α (TNF-α) and IL-6, but not IFN-α, production by bone marrow–derived mast cells (BMMCs). BMMCs were stimulated with culture supernatants (sup) from Pam-212 cells treated with or without HSV at multiplicities of infection (MOIs) of 0.1, 1, 10, or 30, or with lipopolysaccharide (LPS; 10 ng ml^{-1}) as a positive control for 24 hours, and assessed for (**a**) TNF-α, (**b**) IL-6, and (**c**) IFN-α production by ELISA. (**d**) β-Hexosaminidase (β-Hex) assay of BMMCs at 1 hour after stimulation with the culture supernatants from Pam-212 cells treated with or without HSV at MOIs of 0.1, 1, or 10 for 24 hours, or with ionomycin (1 μM) for 10 minutes as a positive control. $^{**}P<0.01$ versus results for untreated Pam-212 cells. Data are representative of three independent experiments, showing the means ($n=3$) ± SD.

Figure 1. Mast cell (MC)-deficient mice exhibit increased clinical severity and mortality following cutaneous herpes simplex virus 2 (HSV-2) infection. MC-deficient C57BL/6-$Kit^{W/W\text{-}v}$ mice (white circles) and the corresponding wild-type (WT) C57BL/6-$Kit^{+/+}$ mice (black squares) ($n=8$) were injected intradermally with HSV-2 186 strain (7.5×10^4 PFU) on the right back. (**a**) Survival rates, (**b**) mean clinical scores, (**c**, **d**) representative clinical photos and cross-sections stained with anti-HSV antibody (Ab) or by hematoxylin and eosin (H&E) staining of HSV-infected skins (original magnification ×200, scale bar = 100 μm), (**e**) quantification of the cell infiltrate in **d** throughout 10 high-power fields (HPFs) of view, and (**f**) HSV titers in the skin ($n=3$) measured in plaque assays at the indicated time points after HSV-2 inoculation are shown. gD, glycoprotein D. The results of $Kit^{+/+}$ mice at days 3 and 5 were below the limit of detection. $^{*}P<0.05$ and $^{**}P<0.01$ versus the corresponding WT mice. Data are representative of at least three independent experiments with similar results, showing the means ($n=3$) ± SD.

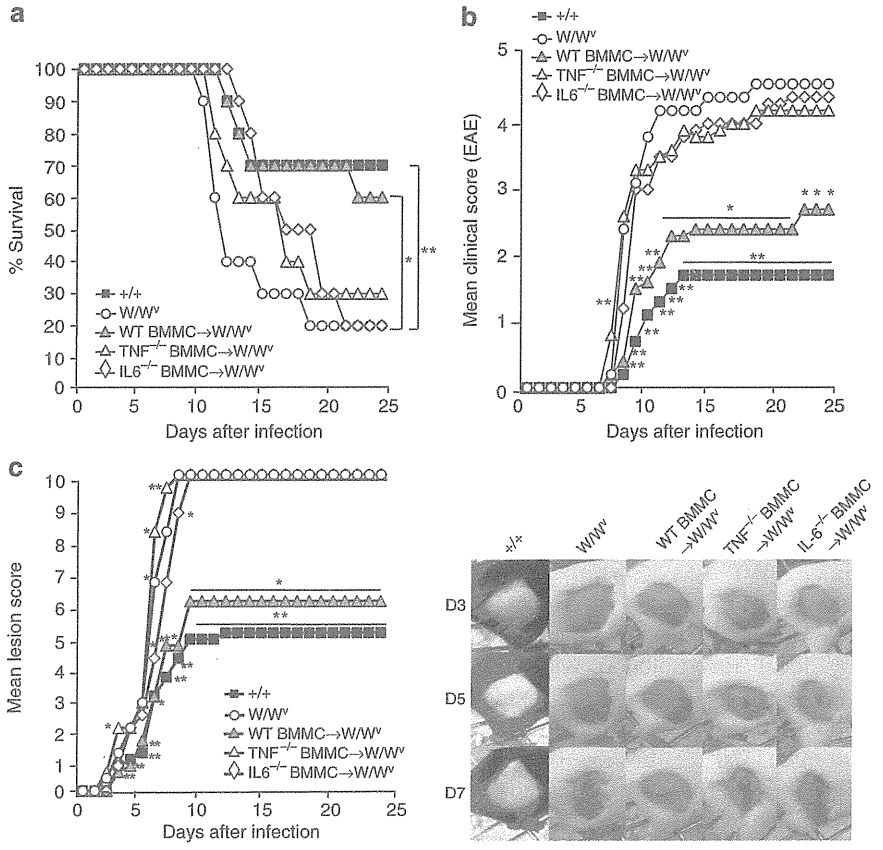

Figure 3. Reconstitution with bone marrow–derived mast cells (BMMCs) derived from wild-type (WT) but not TNF$^{-/-}$ or IL-6$^{-/-}$ mice prevents mortality in Kit$^{W/W\text{-}v}$ mice. (**a**) Survival rates, (**b**) clinical (experimental autoimmune encephalomyelitis (EAE)) scores, (**c**) lesion scores, and representative clinical photographs of skin lesions of Kit$^{W/W\text{-}v}$ mice (white circles), WT Kit$^{+/+}$ mice (black squares), WT BMMC-reconstituted Kit$^{W/W\text{-}v}$ mice (gray circles), TNF$^{-/-}$ BMMC-reconstituted Kit$^{W/W\text{-}v}$ mice (white triangles), and IL6$^{-/-}$ BMMC-reconstituted Kit$^{W/W\text{-}v}$ mice (white lozenges) at the indicated time points after intradermal injection with herpes simplex virus 2 (HSV-2; 7.5×10^4 PFU) are shown. TNF, tumor necrosis factor. $^*P<0.05$ and $^{**}P<0.01$ versus C57BL/6-Kit$^{W/W\text{-}v}$ mice. Data are representative of three independent experiments; $n=10$ mice/group.

we conclude that enhanced TNF-α and IL-6 production in MCs by supernatants from HSV-2-infected keratinocytes is, at least in part, mediated by IL-33 signaling.

MCs do not contribute to the induction of HSV-specific CD8$^+$ T cells

Previous studies revealed a significant role of CD8$^+$ T cells in controlling HSV infections (Simmons and Tscharke, 1992; Chew *et al.*, 2009). Recent studies in mice demonstrated that migrating dermal CD103$^+$ and langerin-expressing DCs are the major transporters of HSV antigens out of skin and, together with resident CD8$^+$ DCs, are the major antigen-presenting cells of HSV antigens to CD8$^+$ T cells in draining lymph nodes (DLNs) (Allan *et al.*, 2003; Bedoui *et al.*, 2009). Therefore, we assessed the number of HSV-gB-specific CD8$^+$ T cells by using tetramer staining, as well as CD8α$^+$ DCs and langerin$^+$ DCs, in DLNs of Kit$^{+/+}$ and Kit$^{W/W\text{-}v}$ mice after intradermal infection with HSV. The proportions of HSV-gB-specific CD8$^+$ T cells in the DLNs of HSV-infected Kit$^{+/+}$ and Kit$^{W/W\text{-}v}$ mice at 6 days after infection were significantly increased when compared with that of uninfected mice (Figure 5a). However, the numbers of HSV-gB-specific CD8$^+$ T cells in Kit$^{+/+}$ and Kit$^{W/W\text{-}v}$ mice were comparable (Figure 5b), suggesting that MCs are not essential for the generation of HSV-specific CD8$^+$ T cells in primary cutaneous HSV-2 infection. Consistent with these findings, there was no significant difference in the frequency of CD8α$^+$ DCs or langerin$^+$ DCs in DLNs of Kit$^{+/+}$ and Kit$^{W/W\text{-}v}$ mice at 2 or 5 days after infection, respectively (Figure 5c). Similarly, no significant difference was detected in the number of CD4$^+$ CD25$^+$ Foxp3$^+$ regulatory T cells found in DLNs (Figure 5d). These results suggest that the impaired clearance of HSV-2 at the infection site observed in Kit$^{W/W\text{-}v}$ mice (Figure 1e) may not be attributed to the impaired induction of HSV-specific cytotoxic T lymphocytes (CTLs).

DISCUSSION

In this study, we have identified previously unknown functions of skin MCs in host protection against HSV-2. The contribution of MCs to host defense against HSV, one of the most common viral infections in the world, had been less clear, probably because MCs are resistant to HSV-2 infection. Indeed, recent

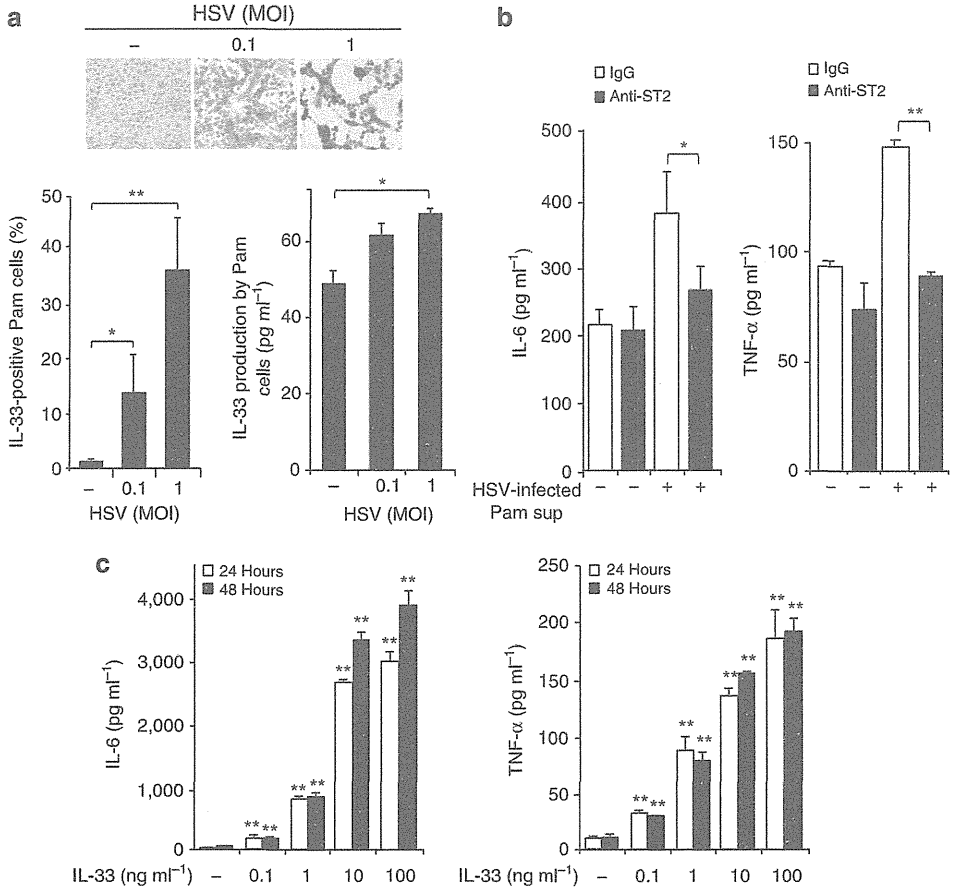

Figure 4. IL-33 is upregulated in herpes simplex virus 2 (HSV-2)–infected keratinocytes, and promotes IL-6 and tumor necrosis factor-α (TNF-α) production by mast cells (MCs). (**a**) Immunohistochemical staining for IL-33 in HSV-infected (multiplicities of infection (MOIs) 0.1 and 1) or uninfected Pam-212 cells 24 hours after infection (original magnification × 400). The percentage of IL-33-positive staining cells in the total population of Pam-212 cells was assessed throughout five high-power fields of view. IL-33 production by HSV-infected (MOIs 0.1 and 1) or uninfected Pam-212 cells 24 hours after infection. (**b**) Bone marrow–derived MCs (BMMCs) were pretreated with anti-T1/ST2 antibody or control IgG for 30 minutes, and then stimulated with culture supernatants (sup) from HSV-infected (MOI 30) or uninfected Pam-212 cells for 24 hours. (**c**) BMMCs were stimulated with control IgG (100 ng ml^{-1}), IL-33 (0.1–100 ng ml^{-1}), or lipopolysaccharide (LPS; 10 ng ml^{-1}) for 24 or 48 hours. (**b**, **c**) IL-6 and TNF-α production by BMMCs was assessed by ELISA. *$P<0.05$ and **$P<0.01$ versus results for control IgG. Data are representative of three independent experiments, showing the means ($n=3$) ± SD.

studies have shown MC involvement in viral host defense, in which the infection of MCs with the virus, such as dengue virus or vaccina virus, is required for MC-mediated immune responses (St John *et al.*, 2011; Wang *et al.*, 2012). Unlike these viral infection models, we demonstrated that MCs are critically involved in viral host defense against HSV-2, even though relatively few HSV-2-infected MCs were detected *in vitro* and *in vivo* (Supplementary Figure S3a online and data not shown). We also report that MC deficiency resulted in impaired HSV-2 clearance at the infection sites during the first 72 hours after infection, suggesting that MCs have key roles as the first line of defense against HSV-2 rather than contributing to acquired immunity. Using "MC knock-in mouse" model, we also demonstrated the crucial contribution of MC-produced TNF-α and IL-6 to protective antiviral responses to HSV-2. Several previous studies suggested an antiviral mechanism involving TNF-α and IL-6 that is responsible for a direct reduction in viral replication or for increasing local infiltration of innate immune cells at the site of HSV infection (Feduchi *et al.*, 1989; Rossol-Voth *et al.*, 1991; Heise and Virgin, 1995; Lundberg *et al.*, 2007; Murphy *et al.*, 2008). In addition, the infiltrating cells, including plasmacytoid DCs, neutrophils, and NK cells, and their products including key antiviral cytokines IFN-α/β, may also provide other means of limiting HSV replication and eliminating virus-infected cells (Melchjorsen *et al.*, 2009).

A recent study revealed that MC-dependent CTL responses are important for an optimized host defense, such as protection against intracellular bacteria, because MCs can internalize, process, and present bacterial antigens and induce antigen-specific activation and proliferation of CD8$^+$ T cells upon infection with *Listeria monocytogenes* (Stelekati *et al.*, 2009). In our model of cutaneous HSV-2 infection, however, HSV-specific CTL generation in MC-deficient mice was not impaired. It is possible that differences in pathogens or their infection levels in MCs might explain the differences in MC

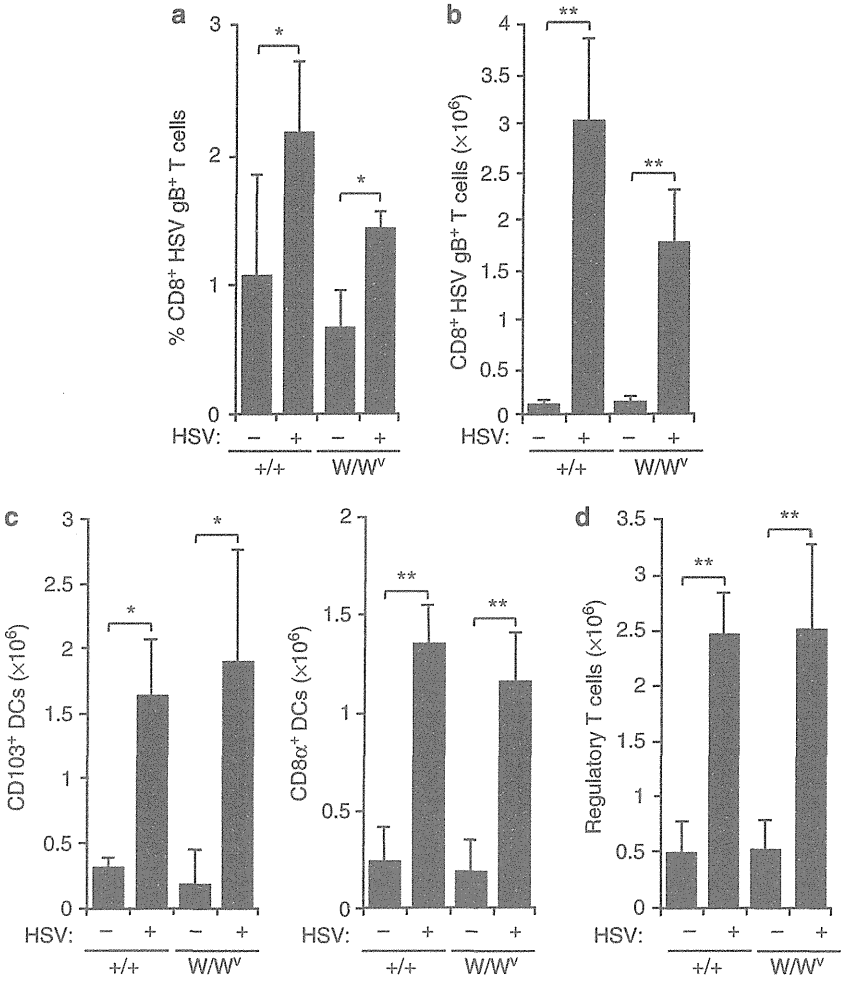

Figure 5. Mast cells (MCs) are not essential for the generation of herpes simplex virus 2 (HSV)–specific CD8$^+$ T cells. Kit$^{W/W\text{-}v}$ and Kit$^{+/+}$ mice were injected with HSV-2, as described in Figure 1. Draining lymph nodes (DLNs) were harvested at (**a**, **b**) 6, (**c**) 2 or 5, and (**d**) 3 days after infection. (**a**) The percentages of CD8$^+$ HSV gB$^+$ T cells in DLNs of HSV-2-infected and -uninfected mice were analyzed by flow cytometry using major histocompatibility complex (MHC) class I tetramer specific for HSV peptide glycoprotein B (gB) or tyrosinase-related protein 2 (TRP2) as a negative control (data not shown). (**b**) The number of CD8$^+$ HSV gB$^+$ T cells in DLNs. (**c**) The number of CD103$^+$ CD205$^+$ dendritic cells (DCs) at 5 days after infection and CD8α$^+$ DCs at 2 days after infection in DLNs. (**d**) The number of CD4$^+$ CD25$^+$ Foxp3$^+$ regulatory T-cell population in DLNs. $^*P<0.05$ and $^{**}P<0.01$ versus the corresponding uninfected mice. Data are representative of two independent experiments, showing the means ($n=5$ mice/group) ± SD.

contribution for CTL generation among these infection models. Nevertheless, in our model, it is still possible that MCs are involved in the recruitment of CTLs to the sites of HSV infection, because CD8$^+$ T-cell recruitment to sites of infection is facilitated by MCs during infection with Newcastle disease virus (Orinska *et al.*, 2005). Further detailed analysis under different viral infection is needed to reveal the functions and significance of MCs for CTL responses against viral infection.

The results of our study show that IL-33 derived from epidermal keratinocytes damaged by viral infection has a critical role in triggering the production of inflammatory cytokines by MCs. Although several viruses have been shown to infect and/or activate MCs *in vitro*, we observe neither significant HSV-2 infection nor HSV-induced direct activation of BMMCs monitored by cytokine production and degranulation. In contrast, the culture supernatants from HSV-2-treated keratinocytes, as well as IL-33 alone, induced TNF-α and IL-6 production by MCs independent of degranulation. The effect of the supernatants from HSV-2-treated keratinocytes was reduced consistently and most effectively by blockade of IL-33–IL-33R signaling in MCs. In addition, although we have recently reported that extracellular adenosine 5′-triphosphate also mediates "danger signal" derived from the damaged keratinocytes (Kawamura *et al.*, 2012), hydrolyzing extracellular adenosine 5′-triphosphate contained in the supernatants by soluble ecto-nucleoside triphosphate diphosphohydrolase (NTPDase; apyrase) did not affect TNF-α and IL-6 production by MCs (data not shown). These results clearly indicate the importance of IL-33 as an "alarmin" in cutaneous HSV infection. Our findings also suggest that IL-33 may be important for other cutaneous virus infections, such as varicella, hand–foot–mouse disease, warts, molluscum, and so on, which also induce the damage or degeneration of

keratinocytes. Further studies are needed to determine whether there is a significant *in vivo* role for IL-33 as an "alarmin" in viral infections other than HSV-2.

MATERIALS AND METHODS

Mice

Female c-Kit-mutant genetically MC-deficient C57BL/6-Kit$^{W/W\text{-}v}$ (Kit$^{W/W\text{-}v}$) mice and the congenic normal C57BL/6-Kit$^{+/+}$ (Kit$^{+/+}$) mice were purchased from Japan SLC (Hamamatsu, Japan). C57BL/6-Kit$^{W\text{-}sh/W\text{-}sh}$ (Kit$^{W\text{-}sh/W\text{-}sh}$) mice were obtained from Sankyo Labo Service (Tokyo, Japan). C57BL/6-Tnf$^{-/-}$ mice and C57BL/6-IL-6$^{-/-}$ mice were purchased from The Jackson Laboratory (Bar Harbor, ME). All animal experiments were carried out in strict accordance with the recommendations in Guidelines for Proper Conduct of Animal Experiments of Science Council of Japan. The protocol was approved by University of Yamanashi Animal Care and Use Committee (permit number: 19–50).

Virus

The WT HSV-2 strain 186 was prepared in Vero cells as described previously (Ushijima *et al.*, 2009), and stored at −80 °C with an approximate titer of 1×10^7 PFU per ml.

HSV inoculation of mice

Kit$^{+/+}$ mice, Kit$^{W/W\text{-}v}$ mice, and Kit$^{W\text{-}sh/W\text{-}sh}$ mice were injected intradermally with HSV-2 (7.5×10^4–7.5×10^5 PFU in 50 μl of EMEM; Nissui, Tokyo, Japan) on the right lower flank after shaving under diethyl ether anesthesia. Mice were then monitored for survival and scored for skin lesions and paralysis. Clinical score was assessed using the experimental autoimmune encephalomyelitis score, and skin lesions were scored as described previously (Takasaki *et al.*, 2000).

Measurement of viral titers and cytokines in HSV-2-inoculated skin

Kit$^{W/W\text{-}v}$ mice or Kit$^{+/+}$ mice were intradermally infected with 7.5×10^4 PFU of HSV-2 186 strain ($n=3$) on the right back. The primary inoculation site of skin (8 × 8 mm) was excised at 1, 3, 5, or 7 days after infection, respectively. Skin samples were thawed and homogenized in 2 ml of Dulbecco's phosphate-buffered saline (Invitrogen, Carlsbad, CA) containing protease inhibitors (Thermo Scientific, Waltham, MA) with sea sand on ice, centrifuged at 7,000 r.p.m. for 5 minutes, and the supernatants were added on Vero cell monolayers. After 24 hours, cultures were fixed with 5% formalin, stained with 0.05% crystal violet, and plaques were counted using a dissecting microscope. For measurement of cytokines, skin samples were excised and homogenized in 250 μl of Tper EDTA-free lysis buffer (Pierce) containing protease inhibitors (Thermo Scientific). Cytokine screening was performed in the supernatants using the Multi-Analyte ELISArray Kit (SABiosciences, Fredrick, MD) according to the manufacturer's instructions.

Preparations of BMMCs

BMMCs were prepared from B6 mice BM cell suspensions, as described previously (Matsushima *et al.*, 2004). Briefly, crude BM cells (4×10^5 cells per ml) were cultured in complete RPMI-1640 (Invitrogen) in the presence of murine recombinant IL-3 (10 ng ml^{-1}) and recombinant stem cell factor (10 ng ml^{-1}; PeproTech, Boston, MA). Nonadherent and loosely adherent cells were recovered twice a week, and further expanded in fresh medium for 4 to 6 weeks. The resulting MC preparations contained >95% CD45$^+$ CD117$^+$ cells.

In vitro HSV infection of BMMCs and keratinocytes

For HSV-2 infection of keratinocytes, 1×10^5 Pam-212 keratinocytes were exposed to HSV-2 strain 186 at an MOI of 0.1, 1, 10, or 30 for 1 hour and washed three times. At 24 hours after incubation, the culture supernatants were collected and passed through a filter (Minisart high flow, pore size 0.1 μm; Sartorius Stedim Biotech, Goettingen, Germany) to remove free virus. For HSV-2 infection of MCs, 2×10^5 BMMCs were infected for 1 hour with HSV-2 at an MOI of 0.1, 1, or 10. Following infection, cells were washed three times and then incubated for an additional 24 hours. In some experiments, BMMCs were stimulated with the culture supernatants from Pam-212 cells, treated with or without HSV for 1 hour, or were stimulated with lipopolysaccharide from *E. coli* serotype 0111:B4, containing <1% protein and <1% RNA (10–100 ng ml^{-1}, Sigma-Aldrich, St Louis, MO) for 24 hours, as control. In the blocking experiments, the culture supernatants from HSV-infected (MOI 30) Pam-212 cells were pretreated with 20 μg ml^{-1} of anti-IL-1α (R&D Systems, Minneapolis, MN), IFN-β (Abcam, Cambridge, UK), and thymic stromal lymphopoietin (R&D Systems) mAbs or isotype-matched control IgG mAbs (BD Pharmingen, San Diego, CA) for 15 minutes before addition to BMMCs. For blocking IL-33-mediated signals, BMMCs were preincubated with 40 μg ml^{-1} of anti-T1/ST2 mAb (MABioproducts, Walkerville, MD) or isotype control mAb for 30 minutes before addition of the culture supernatants from HSV-infected Pam-212 cells. BMMCs were stimulated for 6 hours with the supernatants, washed three times, and incubated in their growth medium for an additional 24 hours. In some experiments, BMMCs were stimulated with control IgG (100 ng ml^{-1}), recombinant IL-33 (0.1–100 ng ml^{-1}, R&D Systems), or lipopolysaccharide (10 ng ml) for 24 or 48 hours. The levels of IL-1α, IL-6, TNF-α, IFN-α, IL-12, and IL-17 in the culture supernatants were determined using an ELISA kit (BD Pharmingen and eBiosciences, San Diego, CA) or the Multi-Analyte ELISArray Kit (SABiosciences) according to the manufacturer's instructions.

Degranulation assay

Degranulation was assessed by β-hexosaminidase assay, as described previously (Matsushima *et al.*, 2004). Briefly, the supernatants were incubated with 2.5 mM *p*-nitrophenyl-*N*-acetyl β-D glucosaminide (Sigma-Aldrich) for 90 minutes. The reactions were terminated by 0.4 M glycine, and the colored products were measured using an ELISA plate reader (Molecular Devices, Sunnyvale, CA).

Local MC reconstitution in Kit$^{W/W\text{-}v}$ mice

Four-week-old Kit$^{W/W\text{-}v}$ mice were transfused by intradermal injection with 2×10^6 BMMCs in 50 μl of RPMI derived from Kit$^{+/+}$, Tnf$^{-/-}$, or Il-6$^{-/-}$ mice as previously described (Grimbaldeston *et al.*, 2007). At 9 weeks after intradermal transfer, the BMMC-reconstituted Kit$^{W/W\text{-}v}$ mice were used for experiments.

Flow cytometry

Cells were stained with allophycocyanin (APC)-labeled anti-CD3, FITC- or phycoerythrin (PE)-anti-CD8, APC-anti-CD11c, FITC-anti-CD205, and PE-anti-CD103 mAbs (10 μg ml^{-1}, Pharmingen, San Diego, CA) for 30 minutes at 4 °C and analyzed on a FACSCalibur

(Becton Dickinson, Franklin Lakes, NJ). For tetramer staining, inguinal and axillary lymph nodes at 6 days after infection were stained with PE-H-2K^b HSV-1gB498-505 (SSIEFARL) tetramer, or PE-H-2K^b TRP2 tetramer (5 μg ml^{-1}, MBL, Nagoya, Japan) as control, for 20 minutes at 4 °C. To detect regulatory T cells or HSV-2-infected BMMCs, cells were fixed and permeabilized with Cytofix/Cytoperm reagents (BD Biosciences-Pharmingen), and then stained with APC-anti-Foxp3 mAb using the Foxp3 Staining Set (eBioscience) or FITC-anti-HSV glycoprotein D mAb (Argene, Verniolle, France), respectively.

Immunohistochemistry

Skin tissues were collected from infected sites at 1, 3, or 5 days after HSV infection and fixed in formalin. Paraffin-embedded sections were dewaxed and rehydrated through graded concentrations of ethanol. Tissue sections were stained with hematoxylin–eosin. Otherwise, the sections were preincubated with 3% hydrogen peroxide in methanol for 10 minutes to inactive endogenous peroxidase. Sections were incubated with rabbit anti-HSV-2 polyclonal antibody or control rabbit Ig for 1 hour at room temperature using the Dako envision kit (Dako, Glostrup, Denmark). The sections were washed and incubated with a goat anti-rabbit Ig conjugated to peroxidase-labeled dextran polymer for 1 hour at room temperature. After wash, they were treated with the chromogenic indicator dye 3,3′-diaminobenzidine for 5 minutes, and then counterstained with Mayer's hematoxylin. For IL-33 staining, plated Pam-212 cells exposed to HSV for 24 hours were washed and stained with goat anti-mouse IL-33 polyclonal antibody (R&D Systems) at 10 μg ml^{-1} for 3 hours at room temperature using the Dako LSAB kit (Dako). Cells were incubated with biotinylated anti-goat secondary antibody, and then incubated with peroxidase-conjugated streptavidin for 30 minutes. After development with 3,3′-diaminobenzidine substrate, cells were counterstained with Mayer's hematoxylin.

Statistical analyses

The GraphPad Prism 5 software (GraphPad Software, La Jolla, CA) was used to determine the statistical significance of survival data. Log-rank test was used for comparison of survival curves. Other data were analyzed by Student's *t*-test.

CONFLICT OF INTEREST

The authors state no conflict of interest.

ACKNOWLEDGMENTS

We thank Kazutoshi Harada and Naotaka Shibagaki for their helpful discussions, Hajime Suto for Kit$^{W\text{-}sh/W\text{-}sh}$ mice, and Miyuki Ogino for technical assistance. These studies were supported in part by a grant from the Ministry of Education and Science of the Japanese Government (grant 10377541, http://kaken.nii.ac.jp). The funder had no role in study design, data collection and analysis, decision to publish, or preparation of the manuscript.

SUPPLEMENTARY MATERIAL

Supplementary material is linked to the online version of the paper at http://www.nature.com/jid

REFERENCES

Abraham SN, St John AL (2010) Mast cell-orchestrated immunity to pathogens. *Nat Rev Immunol* 10:440–52

Allan RS, Smith CM, Belz GT *et al.* (2003) Epidermal viral immunity induced by CD8alpha+ dendritic cells but not by Langerhans cells. *Science* 301:1925–8

Bedoui S, Whitney PG, Waithman J *et al.* (2009) Cross-presentation of viral and self antigens by skin-derived CD103+ dendritic cells. *Nat Immunol* 10:488–95

Bonilla WV, Frohlich A, Senn K *et al.* (2012) The alarmin interleukin-33 drives protective antiviral CD8 T cell responses. *Science* 335:984–9

Chang YJ, Kim HY, Albacker LA *et al.* (2011) Innate lymphoid cells mediate influenza-induced airway hyper-reactivity independently of adaptive immunity. *Nat Immunol* 12:631–8

Cheng H, Tumpey TM, Staats HF *et al.* (2000) Role of macrophages in restricting herpes simplex virus type 1 growth after ocular infection. *Invest Ophthalmol Vis Sci* 41:1402–9

Chew T, Taylor KE, Mossman KL (2009) Innate and adaptive immune responses to herpes simplex virus. *Viruses* 1:979–1002

Corey L, Spear PG (1986) Infections with herpes simplex viruses (1). *N Engl J Med* 314:686–91

Dawicki W, Marshall JS (2007) New and emerging roles for mast cells in host defence. *Curr Opin Immunol* 19:31–8

Echtenacher B, Mannel DN, Hultner L (1996) Critical protective role of mast cells in a model of acute septic peritonitis. *Nature* 381:75–7

Feduchi E, Alonso MA, Carrasco L (1989) Human gamma interferon and tumor necrosis factor exert a synergistic blockade on the replication of herpes simplex virus. *J Virol* 63:1354–9

Galli SJ, Kalesnikoff J, Grimbaldeston MA *et al.* (2005) Mast cells as "tunable" effector and immunoregulatory cells: recent advances. *Annu Rev Immunol* 23:749–86

Grimbaldeston MA, Nakae S, Kalesnikoff J *et al.* (2007) Mast cell-derived interleukin 10 limits skin pathology in contact dermatitis and chronic irradiation with ultraviolet B. *Nat Immunol* 8:1095–104

Heise MT, Virgin HWt (1995) The T-cell-independent role of gamma interferon and tumor necrosis factor alpha in macrophage activation during murine cytomegalovirus and herpes simplex virus infections. *J Virol* 69:904–9

Kawamura T, Ogawa Y, Nakamura Y *et al.* (2012) Severe dermatitis with loss of epidermal Langerhans cells in human and mouse zinc deficiency. *J Clin Invest* 122:722–32

Kulka M, Alexopoulou L, Flavell RA *et al.* (2004) Activation of mast cells by double-stranded RNA: evidence for activation through Toll-like receptor 3. *J Allergy Clin Immunol* 114:174–82

Looker KJ, Garnett GP, Schmid GP (2008) An estimate of the global prevalence and incidence of herpes simplex virus type 2 infection. *Bull World Health Organ* 86:805–12

Lundberg P, Welander PV, Edwards CK 3rd *et al.* (2007) Tumor necrosis factor (TNF) protects resistant C57BL/6 mice against herpes simplex virus-induced encephalitis independently of signaling via TNF receptor 1 or 2. *J Virol* 81:1451–60

Luthi AU, Cullen SP, McNeela EA *et al.* (2009) Suppression of interleukin-33 bioactivity through proteolysis by apoptotic caspases. *Immunity* 31: 84–98

Malaviya R, Ikeda T, Ross E *et al.* (1996) Mast cell modulation of neutrophil influx and bacterial clearance at sites of infection through TNF-alpha. *Nature* 381:77–80

Matsushima H, Yamada N, Matsue H *et al.* (2004) TLR3-, TLR7-, and TLR9-mediated production of proinflammatory cytokines and chemokines from murine connective tissue type skin-derived mast cells but not from bone marrow-derived mast cells. *J Immunol* 173:531–41

Melchjorsen J, Matikainen S, Paludan SR (2009) Activation and evasion of innate antiviral immunity by herpes simplex virus. *Viruses* 1:737–59

Metz M, Maurer M (2007) Mast cells–key effector cells in immune responses. *Trends Immunol* 28:234–41

Metz M, Siebenhaar F, Maurer M (2008) Mast cell functions in the innate skin immune system. *Immunobiology* 213:251–60

Moussion C, Ortega N, Girard JP (2008) The IL-1-like cytokine IL-33 is constitutively expressed in the nucleus of endothelial cells and epithelial cells in vivo: a novel 'alarmin'? *PLoS One* 3:e3331

Murphy EA, Davis JM, Brown AS *et al.* (2008) Effect of IL-6 deficiency on susceptibility to HSV-1 respiratory infection and intrinsic macrophage antiviral resistance. *J Interferon Cytokine Res* 28:589–95

Orinska Z, Bulanova E, Budagian V *et al.* (2005) TLR3-induced activation of mast cells modulates CD8+ T-cell recruitment. *Blood* 106:978–87

Rossol-Voth R, Rossol S, Schutt KH *et al.* (1991) In vivo protective effect of tumour necrosis factor alpha against experimental infection with herpes simplex virus type 1. *J Gen Virol* 72(Pt 1):143–7

Simmons A, Tscharke DC (1992) Anti-CD8 impairs clearance of herpes simplex virus from the nervous system: implications for the fate of virally infected neurons. *J Exp Med* 175:1337–44

Stelekati E, Bahri R, D'Orlando O *et al.* (2009) Mast cell-mediated antigen presentation regulates CD8+ T cell effector functions. *Immunity* 31: 665–76

St John AL, Rathore AP, Yap H *et al.* (2011) Immune surveillance by mast cells during dengue infection promotes natural killer (NK) and NKT-cell recruitment and viral clearance. *Proc Natl Acad Sci USA* 108:9190–5

Takasaki I, Andoh T, Shiraki K *et al.* (2000) Allodynia and hyperalgesia induced by herpes simplex virus type-1 infection in mice. *Pain* 86:95–101

Ushijima Y, Goshima F, Kimura H *et al.* (2009) Herpes simplex virus type 2 tegument protein UL56 relocalizes ubiquitin ligase Nedd4 and has a role in transport and/or release of virions. *Virol J* 6:168

Wang Z, Lai Y, Bernard JJ *et al.* (2012) Skin mast cells protect mice against vaccinia virus by triggering mast cell receptor S1PR2 and releasing antimicrobial peptides. *J Immunol* 188:345–57

Journal of Bioscience and Bioengineering
VOL. xx No. xx, 1–7, 2013

ELSEVIER

www.elsevier.com/locate/jbiosc

REVIEW

Single-cell-based breeding: Rational strategy for the establishment of cell lines from a single cell with the most favorable properties

Nobuo Yoshimoto and Shun'ichi Kuroda*

Graduate School of Bioagricultural Sciences, Nagoya University, Furo-cho, Chikusa, Nagoya, Aichi 464-8601, Japan

Received 11 July 2013; accepted 28 September 2013
Available online xxx

For efficient biomolecule production (e.g., antibodies, recombinant proteins), mammalian cells with high expression rates should be selected from cell libraries, propagated while maintaining a homogenous expression rate, and subsequently stabilized at their high expression rate. Clusters of isogenic cells (i.e., colonies) have been used for these processes. However, cellular heterogeneity makes it difficult to obtain cell lines with the highest expression rates by using single-colony-based breeding. Furthermore, even among the single cells in an isogenic cell population, the desired cell properties fluctuate stochastically during long-term culture. Therefore, although the molecular mechanisms underlying stochastic fluctuation are poorly understood, it is necessary to establish excellent cell lines in order to breed single cells to have higher expression, higher stability, and higher homogeneity while suppressing stochastic fluctuation (i.e., single-cell-based breeding). In this review, we describe various methods for manipulating single cells and facilitating single-cell analysis in order to better understand stochastic fluctuation. We demonstrated that single-cell-based breeding is practical and promising by using a high-throughput automated system to analyze and manipulate single cells.

[**Key words:** Automated single cell analysis and isolation system; Cellular heterogeneity; Biomolecule production; Stem cells; Hybridomas; Chinese hamster ovary cells]

Mammalian cells have been utilized for long time as a resource in the manufacture of biomolecules and biopharmaceuticals. Hybridomas and Chinese hamster ovary (CHO) cells are the most common cells used in this field (1,2). For efficient production of biomolecules using these cells, it is essential to select cells from cell libraries based on their high expression rate, propagate the cells while maintaining a homogeneous expression rate, and stabilize the high expression rate for long-term culture. Cell screenings for conventional methods of addressing these issues (mass production, cellular homogeneity, and cellular stability) have so far only been executed at the colony level (i.e., single-colony-based breeding; Fig. 1A). Candidate colonies are initially isolated using selection markers [e.g., drug resistance (3–5), auxotrophy (6,7), reporter gene expression (8–10)], subjected to limiting dilution (11), and then evaluated by immunoassays and/or functional assays to identify the single colonies with the highest expression. Recently, the detection and retrieval of those colonies with the most favorable properties have been performed automatically using the robotic system ClonePix FL (12). This system uses fluorescence-linked immunosorbent assay (FIA) to detect colonies that have the highest expression rates in groups of candidate colonies that are grown in a semi-solid medium. The system then uses a metal capillary to retrieve the colonies. Cell lines are established from the selected colonies by propagation over several passages and further evaluation of the stability of the higher rate of expression.

TWO MAJOR PROBLEMS OF CONVENTIONAL CELL BREEDING

After hybridomas established by the conventional ways are grown by fed-batch culture for more than 80 days, their expression decreased in a culture time-dependent manner (13). In addition, when isogenic IgG-producing CHO cells were separated into two groups (higher and lower IgG production) by fluorescence-activated cell sorter (FACS), the expression levels of both groups converged to that of parental cells after long-term culture (10). These spontaneous changes are considered to be due to the cellular heterogeneity in a selected single colony or stochastic fluctuation that occurs in each cell during long-term culture. Moreover, when single cells from isogenic hybridomas grow into single colonies of more than 4 cells, each colony has distinct levels of antibody expression because of stochastic fluctuation during the early phase of cell growth (14). Therefore, for effective establishment of cell lines, it is crucial to isolate single cells that have the highest expression rate as quickly as possible, and then propagate them homogeneously while minimizing the stochastic fluctuation (i.e., single-cell-based breeding; Fig. 1B). However, single cells cannot be manipulated in a high-throughput manner using conventional techniques. This makes it difficult to minimize cellular heterogeneity and determine the

* Corresponding author. Tel./fax: +81 52 789 5227.
E-mail address: skuroda@agr.nagoya-u.ac.jp (S. Kuroda).

1389-1723/$ – see front matter © 2013, The Society for Biotechnology, Japan. All rights reserved.
http://dx.doi.org/10.1016/j.jbiosc.2013.09.016

Please cite this article in press as: Yoshimoto, N., and Kuroda, S., Single-cell-based breeding: Rational strategy for the establishment of cell lines from a single cell with the most favorable properties, J. Biosci. Bioeng., (2013), http://dx.doi.org/10.1016/j.jbiosc.2013.09.016

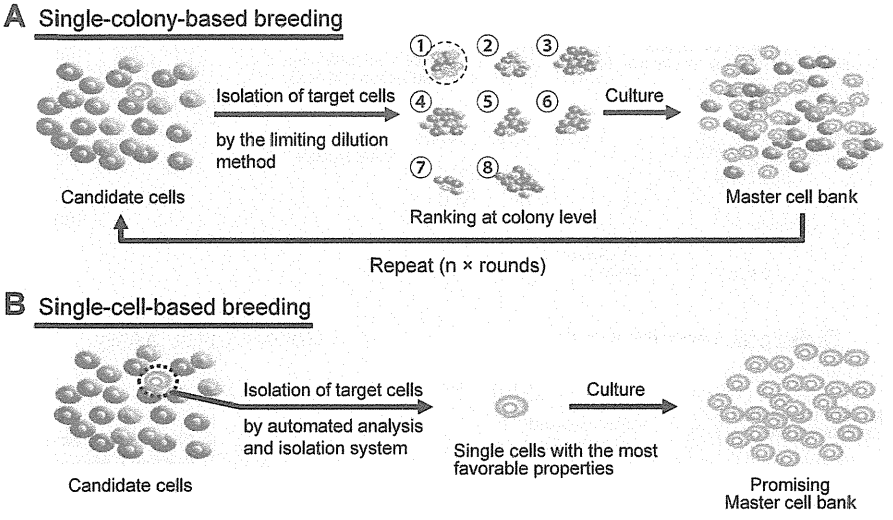

FIG. 1. Comparison of single-colony-based breeding (conventional) method with single-cell-based breeding (new) method. (A) Single-colony-based breeding. Candidate cells were divided into single cells by the limiting dilution method, and allowed to form colonies. Each colony was ranked based on the degree of favorable properties (light green cell showed the most favorable properties). Numbers in circles indicate the rank order of each colony. Top-ranked colony was further propagated to establish master cell bank, which was still contaminated with cells with non-favorable properties. The breeding process should be repeated *n* times to maximize the abundance of cells with favorable properties. The process is time-consuming and laborious. (B) Single-cell-based breeding. By using an automated single cell analysis and isolation system, cell showing the most favorable properties was isolated as a single colony. The cell was further propagated to establish master cell bank, which was completely devoid of the contamination of cells with non-favorable properties. Theoretically, it is not necessary to repeat the breeding process. (For interpretation of the references to color in this figure legend, the reader is referred to the web version of this article.)

molecular mechanisms that underlie stochastic fluctuation in specific single cells. On the other hand, substantial numbers of mammalian cell lines that were created by single-colony-based breeding for industrial production of biomolecules have been incidentally found to possess excellent mass productivity, cellular homogeneity, and cellular stability. This strongly suggests that the stochastic fluctuation was successfully suppressed in spite of the lack of precise knowledge about its mechanism. An automated system for manipulating single cells in a high-throughput manner that could identify single cells with the most favorable properties from huge number of candidate cells and isolate single cells of interest automatically would facilitate the refinement of cell breeding. This innovative approach would solve the problem of cellular heterogeneity, lead to the deciphering of the mechanisms of individual cell stochastic fluctuation, and facilitate the effective establishment of biomolecule-producing cells with high expression, homogeneity, and stability.

Here, we will provide an overview of the current techniques for single-cell analysis and isolation, and introduce an automated single-cell analysis and isolation system that we developed for single-cell-based breeding. We will also describe how to refine cell breeding using this system, and discuss the potential of this rational and reliable methodology for cell-based research and industry.

CURRENT TECHNIQUES FOR IDENTIFYING SINGLE CELLS WITH THE HIGHEST SECRETION RATE

To select single cells that secrete relatively large amounts of biomolecules, candidate cells in a cell library were often fluorescently labeled according to their secretion rates, and then subjected to fluorescent measurement, and single-cell isolation. This process requires nascent biomolecules to be retained within cell bodies by treating them with brefeldin A and labeling them with fluorophores, which severely affects cell viability and prevents the isolated cells from producing biomolecules. To accomplish single-cell-based breeding in a non-destructive, high-yield, and high-throughput manner, a reporter gene that encodes a fluorescent protein is introduced into the biomolecule gene using an internal ribosome entry site (IRES) (8). This allows the fluorescent measurement of the expression rate of each cell (Fig. 2A). However, this bicistronic reporter assay requires additional genetic modification and directly evaluates the synthesis rate of biomolecules, not their secretion rate. Gel microdrop assays have been used to measure secretion. For this assay, candidate cells are grown in a solid-medium containing biotinylated agarose, streptavidin, and biotinylated capture antibody. The cells are then formulated into gel microdrops, and placed in contact with fluorescence-labeled detection antibodies. The secreted biomolecules of each cell are then immobilized in the agarose matrix of the gel microdrop and form fluorescence-labeled immunocomplexes (Fig. 2B) (15). This method can be adapted to high-throughput isolation of efficient biomolecule-producing cells in a secretion-dependent manner, but both low encapsulation efficiency of cells (<15% of gel microdrops) and the physical stress caused by the solid medium remain to be addressed. Moreover, to avoid the encapsulation of cells into gel microdrops, the cell surface is initially coated with semi-solid medium, chemically labeled with biotin, and then mixed with neutravidin and biotinylated capture antibody. Secreted biomolecules immobilized as an immunocomplex in the vicinity of cells are detected by fluorescence-labeled detection antibody. This assay is known as the matrix-based secretion assay (Fig. 2C) (16). Although this assay is more efficient than the gel microdrop assay, the cells still suffer from chemical stress caused by direct biotinylation. More recently, a cell-surface fluorescence-linked immunosorbent assay (CS-FIA) was developed to measure the amount of nascent biomolecules secreted from single cells in a non-destructive manner (17). After the surface of candidate cells is modified with non-toxic lipid-labeled capture antibodies, nascent secreted antibodies are captured on the cell surface and subsequently detected with fluorescence-labeled detection antibodies (Fig. 2D). This method can be used to measure the amount of captured antibodies with extremely high sensitivity (from 6.25 fg/cell to 6.40 pg/cell). CS-FIA is a promising and reliable non-destructive and high-throughput method for identifying the individual cells that most efficiently secrete biomolecules.

Please cite this article in press as: Yoshimoto, N., and Kuroda, S., Single-cell-based breeding: Rational strategy for the establishment of cell lines from a single cell with the most favorable properties, J. Biosci. Bioeng., (2013), http://dx.doi.org/10.1016/j.jbiosc.2013.09.016

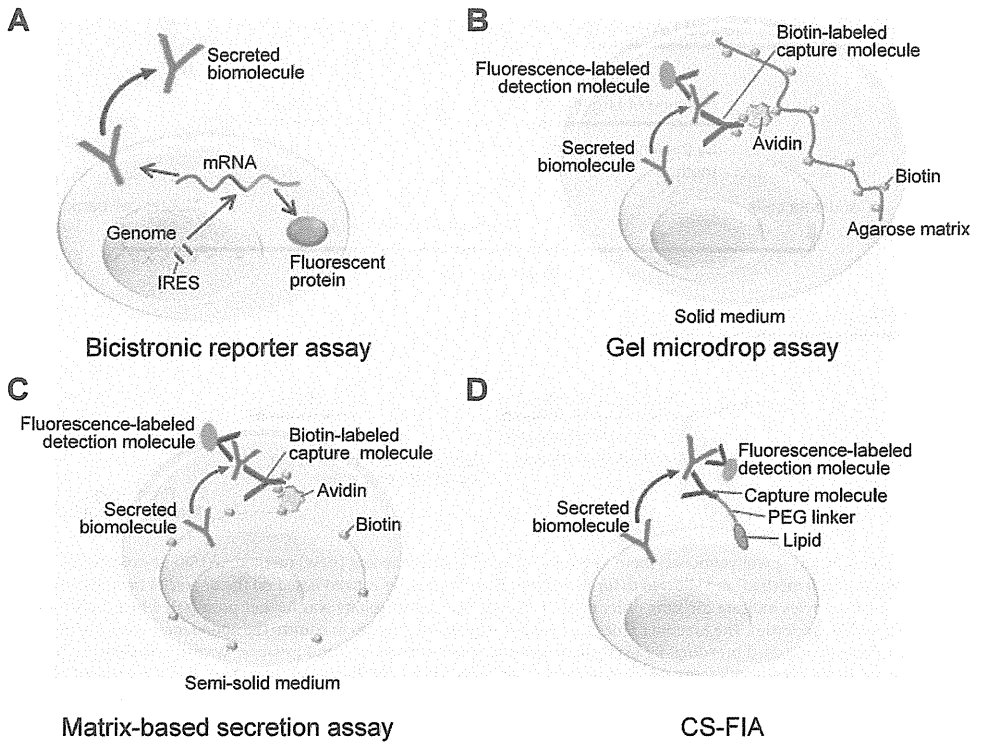

FIG. 2. Fluorescence-labeling techniques for single cells in a biomolecule secretion level-dependent manner. (A) Bicistronic reporter assay. A fluorescent protein gene was placed under the biomolecule gene of expression cassette by using internal ribosome entry site (IRES). This assay allows real-time measuring the transcription level of biomolecule gene in each cell, not always reflecting the secretion level. (B) Gel microdrop assay. Each cell was encapsulated in a solid medium microdrop containing biotinylated agarose, avidin, and biotin-labeled capture molecule. Biomolecules secreted from each cell were immobilized on the agarose matrix, and then sandwiched with fluorescence-labeled detection molecules. Fluorescence intensity of each cell increases in proportion to the secretion rate of biomolecules from each cell. (C) Matrix-based secretion assay. Surface of each cell was chemically labeled with biotin, and then each cell was encapsulated in a semi-solid medium containing avidin and biotin-labeled capture molecules. Secreted biomolecules were immobilized with biotin-labeled capture molecules at cell surface, and then sandwiched with fluorescence-labeled detection molecules. Fluorescence intensity of each cell increases in proportion to the secretion rate of biomolecules from each cell. (D) Cell-surface fluorescence-linked immunosorbent assay (CS-FIA). Each cell was incubated with lipid-PEG (polyethylene glycol)-labeled capture molecules for displaying the moiety of capture molecules onto cell surface spontaneously. Secreted biomolecules were immobilized with capture molecules at cell surface, and then sandwiched with fluorescence-labeled detection molecules. Fluorescence intensity of each cell increases in proportion to the secretion rate of biomolecules from each cell.

CONVENTIONAL TECHNIQUES FOR SINGLE-CELL ANALYSIS AND ISOLATION

The limiting dilution method has long been used to generate single colonies from single cells in order to isolate single cells with favorable properties (e.g., the highest synthesis and secretion rate of biomolecules). Candidate cells are serially diluted in multi-well plates so that each well contains approximately 1 cell. The cells then undergo long-term culture (3–7 days) for colony formation. Either supernatant or cell lysate of each colony is then subjected to enzyme-linked immunosorbent assay (ELISA) or to a functional assay in order to rank the colonies by according to the degree of favorable properties (e.g., productivity of biomolecules) (see nos. 1–8 with circle in Fig. 1A). Because the cells within a colonies are often heterogeneous, limiting dilution should be repeated until a colony with low cellular heterogeneity is obtained that also has the most favorable properties (14,18). The limiting dilution method is laborious, time-consuming, and unsuitable for high-throughput screening.

FACS, which uses fluorescence as an indicator for the most favorable cell properties, has been widely used for a high-throughput single-cell analysis and isolation in biological and biomedical fields (1). In this method, cells in sheath solution are introduced at high flow velocity ($\sim 10^4$ cells/sec) in a high-pressure flow path ($\sim$70 psi) to align them in a laminar flow formation. Target cells are identified using an optical system based on their fluorescent intensities and are then sorted into reservoir wells using high voltage ($\sim 6 \times 10^3$ V). At least 10^5 cells at a density of 10^5–10^6 cells/ml (19,20) are necessary for FACS analysis. Positive cells should make up more than 0.1% of the candidate cells (21), which is the threshold for discriminating them from background cells spectrophotometrically. Before cell sorting, a portion of the cell sample must be discarded in order to optimize the measurement conditions. Additionally, single cells isolated by FACS generally suffer from chemical stress derived from the sheath solution, mechanical stress from laminar flow formation, and electrical stress from sorting (22,23). These issues render FACS unsuitable for rare cells (less than 10^5 cells), diluted cells (less than 10^5 cells/ml), samples containing less than 0.1% positive cells, and vulnerable cells.

As an alternative to FACS, on-chip flow cytometers have been developed that use microfluidics (24–26). Single cells in a culture medium are flowed at a moderate flow velocity ($\sim 5 \times 10^2$ cells/sec) under atmospheric pressure through a microchannel that is $\sim$80 μm in diameter. The cells of interest are identified by their fluorescent intensities, and are sorted to reservoir wells by weak voltage ($\sim$6 V). Using this method, the processing rate can be increased by increasing the number of microchannels in parallel. This system is suitable for rare cells and vulnerable cells. However, probably due to the failure of cells to align in the microchannels, this system is only able to detect 70% of positive cells in samples (27).

Please cite this article in press as: Yoshimoto, N., and Kuroda, S., Single-cell-based breeding: Rational strategy for the establishment of cell lines from a single cell with the most favorable properties, J. Biosci. Bioeng., (2013), http://dx.doi.org/10.1016/j.jbiosc.2013.09.016

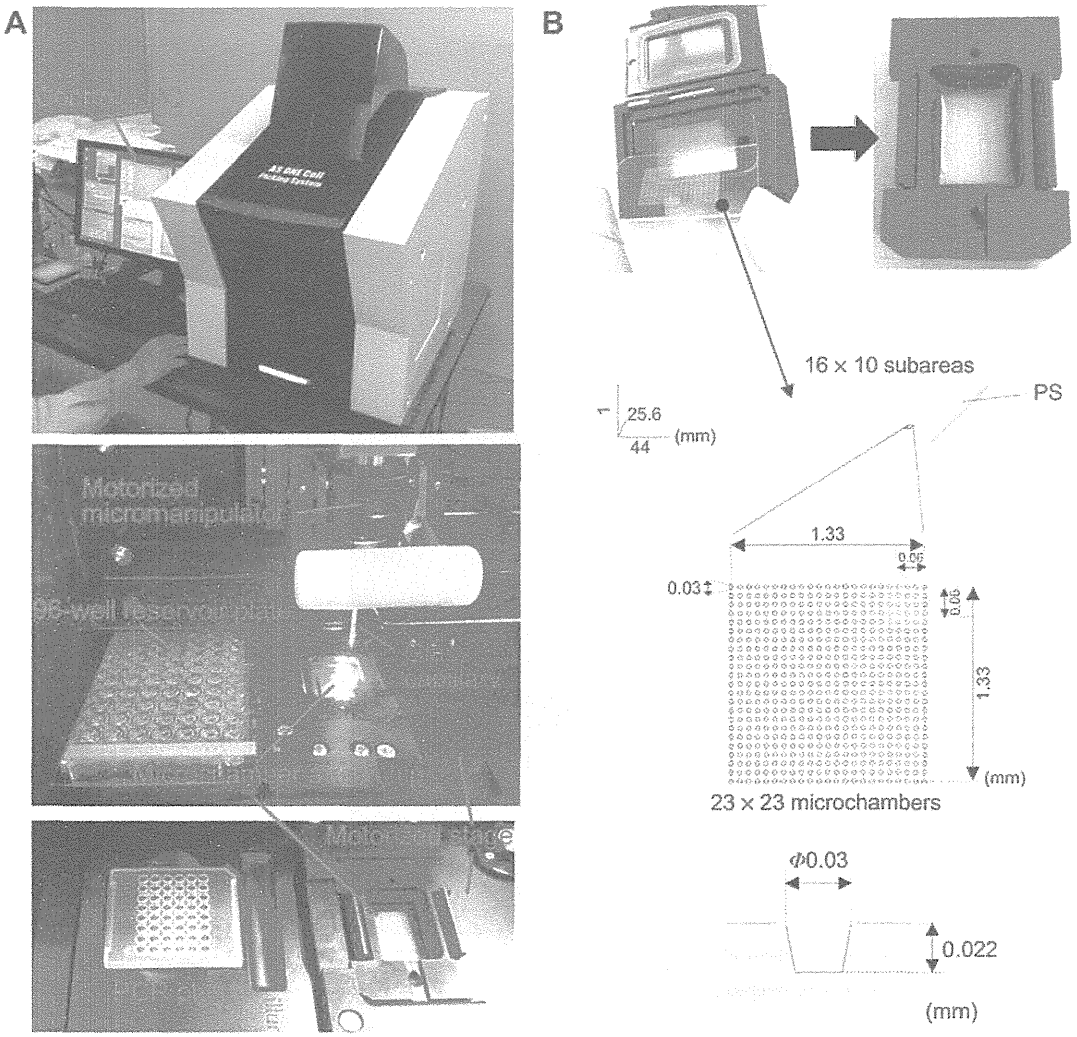

FIG. 3. Automated single-cell analysis and isolation system. (A) Overview of the robot (top). The robot consists of a motorized micromanipulator equipped with a glass capillary, a motorized stage, a reservoir plate (e.g., 6-, 12-, 24-, 48-, 96-, or 384-well format; 48- or 96-well PCR plate), and a microchamber array chip (middle and bottom). (B) Microchamber array chip. A microchamber array chip (1 × 25.6 × 44 mm) made of polystyrene (PS) consists of 16 × 10 subareas, each of which contains 23 × 23 microchambers (30 μm in diameter, 22 μm in depth).

CELL ARRAY SYSTEMS

In cell array systems, each cell is accommodated into a microchamber (10–30 μm in diameter, approximately 2×10^5 microchambers/chip) made of various polymers, such as, polystyrene, polymethylmethacrylate, polydimethylsiloxane, or silicon substrates (21,28,29). These cell arrays are subjected to large-scale analysis of single cells under mild conditions (atmospheric pressure, culture medium). The cells of interest can be detected at the single-cell level with a high signal to noise ratio, which excludes contamination by pseudo-positive cells in the same microchamber. However, because this method involves manual cell isolation is using a micromanipulator, a semi-automated colony isolation system, CellCelector, has been optimized as a single-cell isolation system (30). In this system, one or a few antibody-secreting cells are accommodated into cuboid microchambers (50 μm wide × 50 μm height × 50 μm depths) and covered with a glass slip coated with capturing molecules (anti-IgG antibodies). After removing the glass slip, the secreted antibodies captured on the slip are visualized with fluorescence-labeled secondary antibodies or specific antigens for identifying the cells that secrete antigen-specific antibodies. After matching the positions of the glass slip with those of microchambers, the cells of interest are automatically retrieved from the respective microchambers using a glass capillary. A similar automated single-cell isolation system, Cellporter, has been recently developed (31). When cells in microchambers (10 μm in diameter, 15 μm depths) were stimulated by oxidative or acidic stress, the responsive cells are manually identified by an independent fluorometric system and then each cell is automatically retrieved using a metal capillary. Both CellCelector and Cellporter systems facilitate the isolation of single cells from rare samples (less than 10^5 cells), diluted samples (less than 10^5 cells/ml), samples containing less than 0.1% positive cells, and vulnerable samples. However, both systems still require an additional device for identifying the cells of interest, which significantly reduces their processing capabilities. Therefore, the development of a fully automated system for single-cell analysis and isolation has been eagerly awaited.

AUTOMATED SINGLE-CELL ANALYSIS AND ISOLATION SYSTEM

We recently developed a stand-alone automated system for high-throughput single-cell analysis and isolation (Fig. 3A) (32). This system consists of a motorized stage (for *xy* movements, <1-μm movement accuracy), a motorized micromanipulator (for *z* movement, <0.1-μm movement accuracy), a pencil pump, a glass

Please cite this article in press as: Yoshimoto, N., and Kuroda, S., Single-cell-based breeding: Rational strategy for the establishment of cell lines from a single cell with the most favorable properties, J. Biosci. Bioeng., (2013), http://dx.doi.org/10.1016/j.jbiosc.2013.09.016

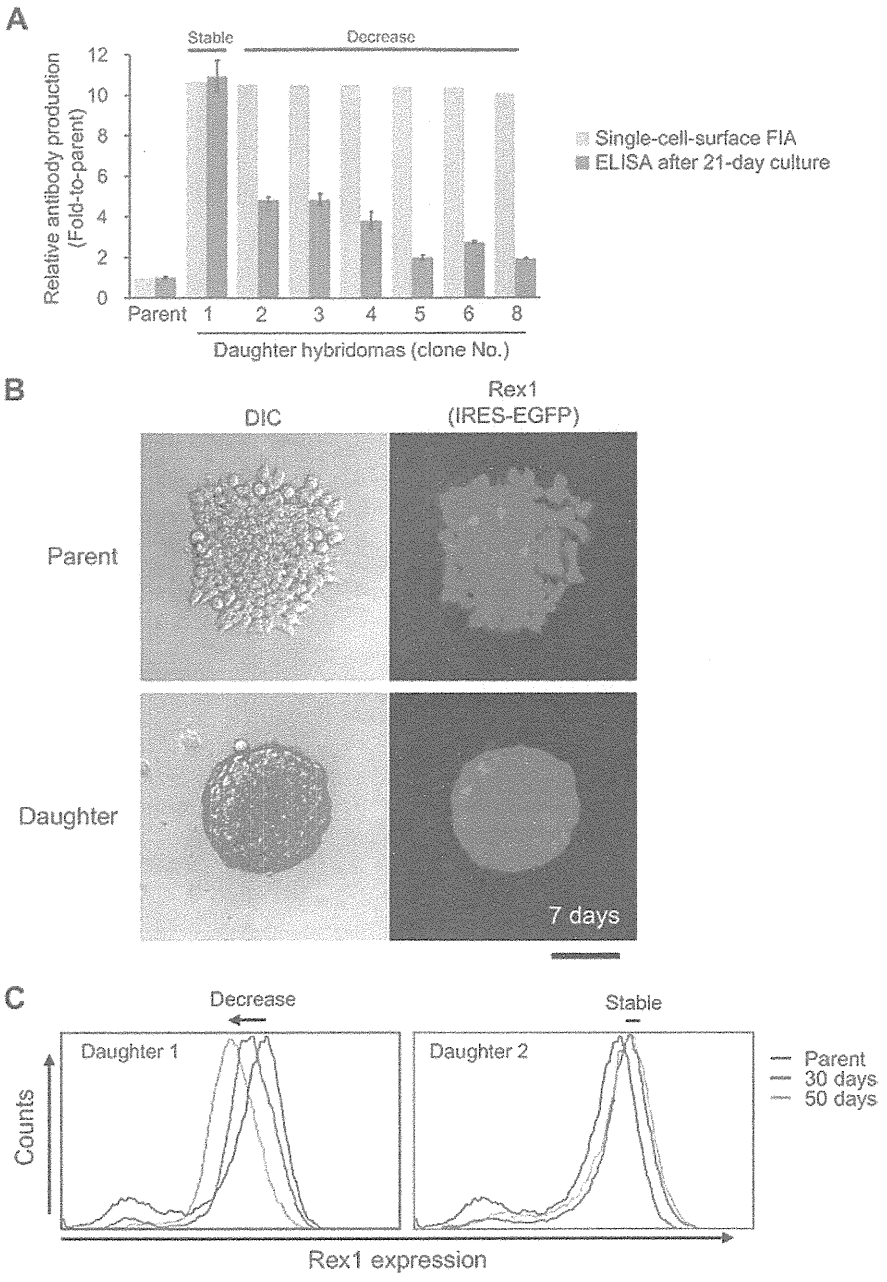

FIG. 4. Single-cell-based breeding of hybridomas and embryonic stem cells. (A) Fluctuation of antibody secretion rate of hybridomas after the propagation from single cells (21 days). Parent hybridomas (antibody secretion was optimized by single-colony-based breeding method) were subjected to CS-FIA (cyan bars), and then single hybridomas showing highest secretion rate (daughter hybridomas) were isolated by the automated single-cell analysis and isolation system. After these hybridomas were propagated for 21 days, culture media were analyzed by ELISA for the determination of secretion rate of antibodies (magenta bars). The antibody secretion rate of clone no. 1 was found stable during at least 21-day culture from single cell isolation, while those of other clones were found to be decreased. Error bars, $p < 0.05$, $n = 6$. (B) Colony formation of single ES cell showing highest expression of pluripotent marker *Rex1* gene. Mouse ES cells harboring *Rex1-IRES-EGFP* gene (parent cells) were subjected to the automated single-cell analysis and isolation system. Single cell showing highest *Rex1* expression (daughter cell) was automatically identified and subsequently isolated by the robot, and cultured to form colony for 7 days. Bars: 50 μm. (C) Fluctuation of pluripotent marker *Rex1* gene expression of daughter ES cells after the propagation from single cells (30 and 50 days). Parent ES cells (*Rex1* gene expression was optimized by single-colony-based breeding method) were subjected to the robot, and then two single cells showing highest *Rex1* gene expression (daughter cells nos. 1 and 2) were isolated by the robot. After the propagation for 30 and 50 days, parental, daughter no. 1, and daughter no. 2 cells were analyzed by FACS for the determination of *Rex1* gene expression. The *Rex1* gene expression of daughter no. 2 was found stable during at least 50-day culture from single cell isolation, while that of daughter no. 1 was found to be decreased.

capillary (40.5 μm inner diameter), fluorescence microscopy equipped with a CCD camera, a reservoir plate (6-, 12-, 24-, 48-, 96-, or 384-well format; 48- or 96-well PCR plate), a microchamber array chip (polystyrene, 30 μm in diameter, 22 μm in depth, 23 × 23 microchambers/subarea, 16 × 10 subareas/chip, 84,640 microchambers/chip; see also Fig. 3B), and a control computer. After fluorometrically scanning all cells in a cell array (excitation at 405 nm, 488 nm, and 633 nm; 7 s/subarea), a histogram of fluorescent intensity from each cell is generated that is used to rank cells in order of fluorescent intensity. Simultaneously, the system generates a list of addresses, fluorescent intensities, and images, including a transmission image of each cell. The cells of interest are identified automatically or manually based on their fluorescent intensities. Microchambers containing more than 2

Please cite this article in press as: Yoshimoto, N., and Kuroda, S., Single-cell-based breeding: Rational strategy for the establishment of cell lines from a single cell with the most favorable properties, J. Biosci. Bioeng., (2013), http://dx.doi.org/10.1016/j.jbiosc.2013.09.016

cells are automatically excluded. Selected cells are promptly retrieved one-by-one using a glass capillary, and are transferred to assigned reservoir wells (10 s/cell). The retrieval of selected cells is confirmed by the elimination of fluorescence in each microchamber. Upon failure, the system automatically repeats the isolation process for the cell. The automated single-cell analysis and isolation system maximizes the usability of cell array systems. Moreover, as the parts that come in contact with samples (i.e., microchamber array chips, glass capillaries, reservoir plates) are essentially disposable, the system significantly reduces the risk of contamination and infection, and is therefore more applicable than conventional cell analysis and isolation systems to research conducted in accordance with good laboratory practices (GLP) and production performed under good manufacturing practices (GMP).

SINGLE-CELL-BASED BREEDING OF HYBRIDOMAS AND EMBRYONIC STEM CELLS

We used the automated single-cell analysis and isolation system to select 362 cells that exhibited higher fluorescence than parental hybridomas from $\sim 5.0 \times 10^4$ hybridomas that were established by conventional methods and subjected to CS-FIA (Fig. 2D). Eight cells with the highest level of fluorescence were isolated by the system, and were further propagated to about $\sim 5.0 \times 10^5$ cells over 2 weeks. Finally, after 21 days of culture, 7 hybridomas were found to secret higher amounts (up to 10-fold) of antibodies than parental hybridomas (Fig. 4A) (32). Hybridoma clone no. 1 was able maintain the high secretion rate without any decrease for at least 35 days. The combination of the automated single-cell analysis and isolation system with CS-FIA was thus demonstrated to be effective and practical for improvement of the productivity of biomolecules that are secreted from various cells.

To establish mouse embryonic stem cells (ESCs) with the highest pluripotency, parental ESCs were firstly modified to incorporate the *EGFP* (enhanced green fluorescent protein) gene under the *Rex1* gene (a pluripotent marker) using a bicistronic reporter system (Fig. 2A). About 1.0×10^5 cells of parental ESCs were subjected to the automated single-cell analysis and isolation system and 25 single cells showing higher fluorescence were isolated. These cells were subsequently cultured for 7 days to form colonies. About 64% (16/25) of daughter cells formed more spherical colonies and exhibited more uniform fluorescence than parental cells (Fig. 4B). Furthermore, after 50 days, some portions of daughter cells were retained stable and high expression of the *Rex1* gene, indicating that the stochastic fluctuation of pluripotency was successfully suppressed by single-cell-based breeding (Fig. 4C). Taken together, the automated single-cell analysis and isolation system may resolve cellular heterogeneity; one of the two major problems that occur during conventional single-colony based breeding (see above). However, it is an indispensable tool for solving the problem of stochastic fluctuation, fully establishing the single-cell-based breeding.

MANAGEMENT OF STOCHASTIC FLUCTUATION FOR SINGLE-CELL-BASED BREEDING

Even among isogenic cells, stochastic fluctuation is often found in epigenetic modification (33,34), protein expression (35–37), transcription (38,39), and cell-cycle progression (40). Single-cell omics analyses of isogenic cells have recently revealed that these stochastic fluctuations occur at the level of individual cells. When cellular heterogeneity is successfully excluded from cell breeding using our system, the established cell lines often have reduced productivity of biomolecules during long-term culture. This might be caused by the stochastic fluctuation that occurs in each cell. To establish single-cell-based breeding, it is necessary to decipher the molecular basis underlying stochastic fluctuation and to thereby identify the master regulators that govern this fluctuation. These postulated regulators could be found using global analyses (e.g., genomics, epigenomics, transcriptomics, proteomics, and metabolomics) of cells with relatively high expression, stability, and homogeneity and using isogenic cells as controls. The use of the regulators as a marker in an automated single-cell analysis and isolation system would significantly increase the likelihood of isolating those cells with relatively low stochastic fluctuation. Furthermore, stochastic fluctuation could be minimized by managing the expression level of the regulators. Indeed, through the single-cell-based breeding of ESCs, Nanog, a pluripotent marker, has been identified as one of the master regulators that can be managed to maintain high pluripotency by suppressing stochastic fluctuation (41).

CONCLUDING REMARKS

In order to obtain the efficient secretion of biomolecules, cell lines should be established that avoid both cellular heterogeneity at the colony level and stochastic fluctuation at the single-cell level. The combination of the automated single-cell analysis and isolation system with CS-FIA allowed us to obtain single cells that efficiently secrete biomolecules, thereby excluding the influence of cellular heterogeneity in the colonies bred from these cells. To establish single-cell-based breeding, global analysis of these cells would be an effective method for identifying master regulators that govern stochastic fluctuation.

ACKNOWLEDGMENTS

This study was supported in part by Adaptable & Seamless Technology Transfer Program through Target-driven R&D (A-STEP) by the Japan Science and Technology Agency (JST) (AS231Z04687F to N.Y., AS2311699F to S.K.), the Program for Promotion of Basic and Applied Researches for Innovations in Bio-oriented Industry (H22-7, BRAIN to S.K.), a Grant-in-Aid for Scientific Research (A) (25242043 to S.K.), the Health Labor Sciences Research Grant from the Ministry of Health Labor and Welfare (to S.K.), and the As One Corporation (to S.K.). We thank Ken-ichi Kimura and Xu Jie (Furukawa), Masato Fujihashi and Masaya Kurokawa (Starlite), and Masahiro Matsushita, Kenji Uemukai, and Tohru Kaneno (As One).

References

1. **Herzenberg, L. A. and de Rosa, S. C.:** Monoclonal antibodies and the FACS: complementary tools for immunobiology and medicine, Immunol. Today, **21**, 383–390 (2000).
2. **Hacker, D. L., de Jesus, M., and Wurm, F. M.:** 25 Years of recombinant proteins from reactor-grown cells – where do we go from here? Biotechnol. Adv., **27**, 1023–1027 (2009).
3. **Wagman, G. H., Testa, R. T., Marquez, J. A., and Weinstein, M. J.:** Antibiotic G-418, a new micromonospora-produced aminoglycoside with activity against protozoa and helminths: fermentation, isolation, and preliminary characterization, Antimicrob. Agents Chemother., **6**, 144–149 (1974).
4. **Southern, P. J. and Berg, P.:** Transformation of mammalian cells to antibiotic resistance with a bacterial gene under control of the SV40 early region promoter, J. Mol. Appl. Genet., **1**, 327–341 (1982).
5. **Blochlinger, K. and Diggelmann, H.:** Hygromycin B phosphotransferase as a selectable marker for DNA transfer experiments with higher eucaryotic cells, Mol. Cell. Biol., **4**, 2929–2931 (1984).
6. **Littlefield, J. W.:** Selection of hybrids from matings of fibroblasts in vitro and their presumed recombinants, Science, **145**, 709–710 (1964).
7. **Simonsen, C. C. and Levinson, A. D.:** Isolation and expression of an altered mouse dihydrofolate reductase cDNA, Proc. Natl. Acad. Sci. USA, **80**, 2495–2499 (1983).
8. **Gurtu, V., Yan, G., and Zhang, G.:** IRES bicistronic expression vectors for efficient creation of stable mammalian cell lines, Biochem. Biophys. Res. Commun., **229**, 295–298 (1996).

Please cite this article in press as: Yoshimoto, N., and Kuroda, S., Single-cell-based breeding: Rational strategy for the establishment of cell lines from a single cell with the most favorable properties, J. Biosci. Bioeng., (2013), http://dx.doi.org/10.1016/j.jbiosc.2013.09.016

9. **Mancia, F., Patel, S. D., Rajala, M. W., Scherer, P. E., Nemes, A., Schieren, I., Hendrickson, W. A., and Shapiro, L.:** Optimization of protein production in mammalian cells with a coexpressed fluorescent marker, Structure, **12**, 1355–1360 (2004).
10. **Pilbrough, W., Munro, T. P., and Gray, P.:** Intraclonal protein expression heterogeneity in recombinant CHO cells, PLoS One, **4**, e8432 (2009).
11. **Lietzke, R. and Unsicker, K.:** A statistical approach to determine monoclonality after limiting cell plating of a hybridoma clone, J. Immunol. Methods, **76**, 223–228 (1985).
12. **Caron, A. W., Nicolas, C., Gaillet, B., Ba, I., Pinard, M., Garnier, A., Massie, B., and Gilbert, R.:** Fluorescent labeling in semi-solid medium for selection of mammalian cells secreting high-levels of recombinant proteins, BMC Biotechnol., **9**, 42 (2009).
13. **Frame, K. K. and Hu, W. S.:** The loss of antibody productivity in continuous culture of hybridoma cells, Biotechnol. Bioeng., **35**, 469–476 (1990).
14. **Gardner, J. S., Chiu, A. L., Maki, N. E., and Harris, J. F.:** A quantitative stability analysis of human monoclonal antibody production by heteromyeloma hybridomas, using an immunofluorescent technique, J. Immunol. Methods, **85**, 335–346 (1985).
15. **Akselband, Y., Moen, P. T., Jr., and McGrath, P.:** Isolation of rare isotype switch variants in hybridoma cell lines using an agarose gel microdrop-based protein secretion assay, Assay Drug Dev. Technol., **1**, 619–626 (2003).
16. **Manz, R., Assenmacher, M., Pflüger, E., Miltenyi, S., and Radbruch, A.:** Analysis and sorting of live cells according to secreted molecules, relocated to a cell-surface affinity matrix, Proc. Natl. Acad. Sci. USA, **92**, 1921–1925 (1995).
17. **Kida, A., Iijima, M., Niimi, T., Maturana, A. D., Yoshimoto, N., and Kuroda, S.:** Cell surface-fluorescence immunosorbent assay for real-time detection of hybridomas with efficient antibody secretion at the single-cell level, Anal. Chem., **85**, 1753–1759 (2013).
18. **Underwood, P. A. and Bean, P. A.:** Hazards of the limiting-dilution method of cloning hybridomas, J. Immunol. Methods, **107**, 119–128 (1988).
19. **Kurimoto, K., Yabuta, Y., Ohinata, Y., and Saitou, M.:** Global single-cell cDNA amplification to provide a template for representative high-density oligonucleotide microarray analysis, Nat. Protoc., **2**, 739–752 (2007).
20. **Ramsköld, D., Luo, S., Wang, Y. C., Li, R., Deng, Q., Faridani, O. R., Daniels, G. A., Khrebtukova, I., Loring, J. F., Laurent, L. C., Schroth, G. P., and Sandberg, R.:** Full-length mRNA-Seq from single-cell levels of RNA and individual circulating tumor cells, Nat. Biotechnol., **30**, 777–782 (2012).
21. **Yamamura, S., Kishi, H., Tokimitsu, Y., Kondo, S., Honda, R., Rao, S. R., Omori, M., Tamiya, E., and Muraguchi, A.:** Single-cell microarray for analyzing cellular response, Anal. Chem., **77**, 8050–8056 (2005).
22. **Ohgushi, M. and Sasai, Y.:** Lonely death dance of human pluripotent stem cells: ROCKing between metastable cell states, Trends Cell Biol., **21**, 274–282 (2011).
23. **Fong, C. Y., Peh, G. S., Gauthaman, K., and Bongso, A.:** Separation of SSEA-4 and TRA-1-60 labelled undifferentiated human embryonic stem cells from a heterogeneous cell population using magnetic-activated cell sorting (MACS) and fluorescence-activated cell sorting (FACS), Stem Cell Rev., **5**, 72–80 (2009).
24. **Takahashi, K., Hattori, A., Suzuki, I., Ichiki, T., and Yasuda, K.:** Non-destructive on-chip cell sorting system with real-time microscopic image processing, J. Nanobiotechnol., **2**, 5 (2004).
25. **Hayashi, M., Hattori, A., Kim, H., Terazono, H., Kaneko, T., and Yasuda, K.:** Fully automated on-chip imaging flow cytometry system with disposable contamination-free plastic re-cultivation chip, Int. J. Mol. Sci., **12**, 3618–3634 (2011).
26. **Fu, A. Y., Spence, C., Scherer, A., Arnold, F. H., and Quake, S. R.:** A microfabricated fluorescence-activated cell sorter, Nat. Biotechnol., **17**, 1109–1111 (1999).
27. **Takao, M. and Takeda, K.:** Enumeration, characterization, and collection of intact circulating tumor cells by cross contamination-free flow cytometry, Cytometry A, **79**, 107–117 (2011).
28. **Jin, A., Ozawa, T., Tajiri, K., Obata, T., Kondo, S., Kinoshita, K., Kadowaki, S., Takahashi, K., Sugiyama, T., Kishi, H., and other 1 author:** A rapid and efficient single-cell manipulation method for screening antigen-specific antibody-secreting cells from human peripheral blood, Nat. Med., **15**, 1088–1092 (2009).
29. **Figueroa, X. A., Cooksey, G. A., Votaw, S. V., Horowitz, L. F., and Folch, A.:** Large-scale investigation of the olfactory receptor space using a microfluidic microwell array, Lab Chip, **10**, 1120–1127 (2010).
30. **Choi, J. H., Ogunniyi, A. O., Du, M., Du, M., Kretschmann, M., Eberhardt, J., and Love, J. C.:** Development and optimization of a process for automated recovery of single cells identified by microengraving, Biotechnol. Prog., **26**, 888–895 (2010).
31. **Suzuki, M., Tanaka, H., and Iribe, Y.:** Detection and collection system of target single cell based on pH and oxygen sensing, J. Robot. Mechatron., **22**, 639–643 (2010).
32. **Yoshimoto, N., Kida, A., Jie, X., Kurokawa, M., Iijima, M., Niimi, T., Maturana, A. D., Nikaido, I., Ueda, H. R., Tatematsu, K., and other 4 authors:** An automated system for high-throughput single cell-based breeding, Sci. Rep., **3**, 1191 (2013).
33. **Obier, N. and Müller, A. M.:** Chromatin flow cytometry identifies changes in epigenetic cell states, Cells Tissues Organs, **191**, 167–174 (2010).
34. **Ben-David, U. and Benvenisty, N.:** The tumorigenicity of human embryonic and induced pluripotent stem cells, Nat. Rev. Cancer, **11**, 268–277 (2011).
35. **Irish, J. M., Kotecha, N., and Nolan, G. P.:** Mapping normal and cancer cell signalling networks: towards single-cell proteomics, Nat. Rev. Cancer, **6**, 146–155 (2006).
36. **Rosenfeld, N., Young, J. W., Alon, U., Swain, P. S., and Elowitz, M. B.:** Gene regulation at the single-cell level, Science, **307**, 1962–1965 (2005).
37. **Cai, L., Friedman, N., and Xie, X. S.:** Stochastic protein expression in individual cells at the single molecule level, Nature, **440**, 358–362 (2006).
38. **Aoi, T., Yae, K., Nakagawa, M., Ichisaka, T., Okita, K., Takahashi, K., Chiba, T., and Yamanaka, S.:** Generation of pluripotent stem cells from adult mouse liver and stomach cells, Science, **321**, 699–702 (2008).
39. **Ko, M. S.:** A stochastic model for gene induction, J. Theor. Biol., **153**, 181–194 (1991).
40. **Symeonidou, I. E., Taraviras, S., and Lygerou, Z.:** Control over DNA replication in time and space, FEBS Lett., **586**, 2803–2812 (2012).
41. **Macarthur, B. D., Sevilla, A., Lenz, M., Müller, F. J., Schuldt, B. M., Schuppert, A. A., Ridden, S. J., Stumpf, P. S., Fidalgo, M., Ma'ayan, A., and other 2 authors:** Nanog-dependent feedback loops regulate murine embryonic stem cell heterogeneity, Nat. Cell Biol., **14**, 1139–1147 (2012).

Please cite this article in press as: Yoshimoto, N., and Kuroda, S., Single-cell-based breeding: Rational strategy for the establishment of cell lines from a single cell with the most favorable properties, J. Biosci. Bioeng., (2013), http://dx.doi.org/10.1016/j.jbiosc.2013.09.016

Analyst

RSC Publishing

PAPER

Nanocapsule-based probe for evaluating the orientation of antibodies immobilized on a solid phase†

Cite this: *Analyst*, 2013, **138**, 3470

Masumi Iijima, Nobuo Yoshimoto, Tomoaki Niimi, Andrés Daniel Maturana and Shun'ichi Kuroda*

The orientation of sensing molecules on solid phase biosensors has to be optimized to facilitate efficient binding of analytes. Since conventional observation methods (*e.g.*, electron microscopy, atomic force microscopy, time-of-flight secondary ion mass spectrometry) require exaggerated machines and possess insufficient resolution for single molecule analyses, functional assays based on the reactivity to analytes have thus far been used for this optimization. However, it is not clear whether these assays can judge whether sensing molecules are fixed in an oriented-immobilization manner or not. Here, we describe that bio-nanocapsules of about 30 nm diameter, displaying approximately 120 molecules of a tandem form of the immunoglobulin (Ig) G Fc-binding Z domain (ZZ-BNCs), can discriminate between the Fc regions of IgGs fixed in an oriented-immobilization manner and those fixed randomly, thus facilitating the evaluation of the orientation of IgGs in immunosensors. Furthermore, in sandwich immunoassays, ZZ-BNCs can bind specifically to detection-IgGs fixed in an oriented-immobilization manner by antigen-capture IgG complexes, rather than to capture-IgGs fixed randomly onto a solid phase, allowing the simultaneous use of the same IgG as capture- and detection-IgGs. Thus, we demonstrate that ZZ-BNCs are a unique probe for evaluating the orientation of IgGs on a solid phase.

Received 11th March 2013
Accepted 13th April 2013

DOI: 10.1039/c3an00481c

www.rsc.org/analyst

Introduction

When developing biosensors, information about the direction, shape, and movement of sensing molecules on a solid phase could significantly contribute to improving the sensitivity, specificity, and analyte-binding capacity. Conventionally, these molecules (especially antibodies) have been analyzed by electron microscopy (EM), atomic force microscopy (AFM), time-of-flight secondary ion mass spectrometry, dual polarization interferometry, neutron reflectometry, and spectroscopic ellipsometry.[1–6] However, for immunosensors, while these methods barely allow direct observation of immunoglobulin (Ig) Gs at a single molecule level, they can neither achieve real-time observation of IgGs in solution nor clearly distinguish Fc from Fab fragments. Recently, by using high-speed AFM, we have succeeded in the real-time observation of IgG molecules on immunosensors in solution,[7] but it is still necessary to optimize the conditions for obtaining a sufficient amount of quantitative data. This situation has led us to evaluate sensing molecules on a solid phase by functional analyses (*e.g.*, reactivity to analytes) using surface plasmon resonance and ellipsometry.[8,9] However, these methods are indeed suitable for the optimization of biosensors, but it is not clear whether they can establish whether sensing molecules are immobilized correctly in an optimal orientation (oriented-immobilization).

On the other hand, sandwich immunoassays have been commonly used for the detection and quantitation of antigens (Ags) in liquid specimens. These systems are useful where Ags are in a crude form or in low concentrations.[10] Capture-IgGs (cIgGs) are passively attached to a solid phase, washed thoroughly with buffer, and then brought into contact with a specimen. Ags are captured by cIgGs on the solid phase, and the cIgG-bound Ags are then detected by IgGs in the aqueous phase (detection-IgGs [dIgGs]) to create a sandwich immunocomplex (cIgG–Ag–dIgG). When detecting the immunocomplex, both cIgGs and dIgGs should be from distinct host species/subclasses, and dIgG-specific secondary antibodies should be used. It is necessary to suppress unexpected cross-reactions between secondary antibodies and cIgGs for the sensitive and specific detection of immunocomplexes on a solid phase. However, if both cIgGs and dIgGs are from the same host species/subclasses, because no molecule has yet been reported that can distinguish dIgGs from cIgGs, dIgGs must be chemically modified with labeling molecules, which often reduce the activity of the dIgGs and hence, the sensitivity of the immunoassay.

We have previously developed bio-nanocapsules (BNCs) of approximately 30 nm diameter by expressing the hepatitis B

Graduate School of Bioagricultural Sciences, Nagoya University, Nagoya, Aichi 464-8601, Japan. E-mail: skuroda@agr.nagoya-u.ac.jp; Fax: +81-52-789-5227; Tel: +81-52-789-5227

† Electronic supplementary information (ESI) available. See DOI: 10.1039/c3an00481c

virus surface antigen (HBsAg) L gene in *Saccharomyces cerevisiae*.[11] BNCs are composed of approximately 110 molecules of HBsAg L proteins embedded within a liposome. Recently, a derivative of BNCs has been generated in which the N-terminal region (amino acids 51–159) of L protein has been replaced with a tandem form of an IgG Fc-binding Z domain derived from *Staphylococcus aureus* protein A;[12] this was designated as ZZ-BNC (Fig. 1A).[13] ZZ-BNCs contain approximately 120 molecules of ZZ-L protein (N-terminally ZZ-fused L protein) and can capture about 60 mouse total IgG molecules and can display all the IgG Fv regions outwardly for effective Ag binding. Thereby, the ZZ-BNCs in aqueous phase could enhance the sensitivity of the immunoassays by cluster formation and oriented-immobilization of 2nd antibodies,[14] and facilitate the simultaneous use of the 1st antibodies derived from same animal species/subclasses.[15] Furthermore, the ZZ-BNCs on a solid phase served as scaffolds for IgGs of immunosensors, and enhanced the Ag-binding capacities and sensitivities by the effect of oriented-immobilization.[16] Thus, since ZZ-BNC displays approximately 240 molecules of an Fc sensor (Z domain) in an oriented-immobilization manner, ZZ-BNCs were expected to show higher avidity for a cluster of Fc fragments rather than for single molecules of an Fc fragment.[17] In this study, unlike our previous studies that utilize ZZ-BNCs as scaffolds for oriented immobilization of IgGs in both aqueous and solid phases, we examined whether ZZ-BNCs *per se* could measure the degree of oriented-immobilization of IgGs on immunosensors and whether ZZ-BNCs could specifically detect dIgGs, as opposed to cIgGs, in sandwich immunoassays.

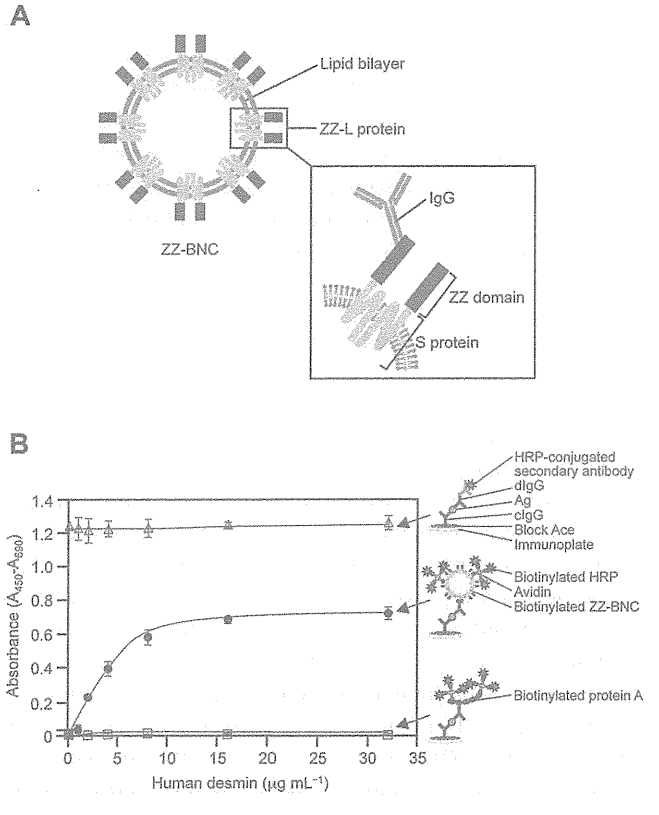

Fig. 1 Sandwich ELISA using ZZ-BNCs. (A) Capsular structure of ZZ-BNC. One ZZ-BNC particle consisted of approximately 120 ZZ-L proteins embedded within a liposome. The ZZ domain and S protein were necessary for the interaction with the IgG Fc region and for particle formation, respectively. (B) Detection of human desmin by sandwich ELISA, using an anti-human desmin mouse monoclonal IgG2a as cIgG and dIgG. The following reagents were added to each well in the indicated order. Open triangles, cIgG (1 μg mL^{-1}), Ag (0–32 μg mL^{-1}), dIgG (1 μg mL^{-1}), and HRP-conjugated goat anti-mouse Fc-specific IgG (secondary antibody) (0.1 μg mL^{-1}); open squares, cIgG (1 μg mL^{-1}), Ag (0–32 μg mL^{-1}), dIgG (1 μg mL^{-1}), biotinylated-protein A (0.1 μg mL^{-1}), and biotinylated-HRP–avidin complex (0.1 μg mL^{-1}); closed circles, cIgG (1 μg mL^{-1}), Ag (0–32 μg mL^{-1}), dIgG (1 μg mL^{-1}), biotinylated-ZZ-BNCs (0.1 μg mL^{-1}), and biotinylated-HRP–avidin complex (0.1 μg mL^{-1}). Schemas for postulated immunocomplexes were represented in the right margin. Results represent the means ± SD (n = 4).

Experimental section

ZZ-BNC

ZZ-BNCs were overexpressed in *Saccharomyces cerevisiae* AH22R$^-$ cells carrying the ZZ-BNC expression plasmid pGLD-ZZ50.[13,18] As described previously,[18] ZZ-BNCs were extracted from yeast cells by disruption with glass beads, heat treated at 70 °C for 20 min, and then purified using AKTA™ (GE Healthcare, Amersham, UK) affinity chromatography with porcine IgG and gel filtration.

Reagents

Recombinant human desmin was purchased from Progen Biotechnik GmbH (Heidelberg, Germany). Chicken IgY was obtained from R&D Systems (Minneapolis, MN, USA) and anti-human desmin mouse monoclonal IgG2a from Abcam (Cambridge, UK). Anti-chicken IgY rabbit polyclonal IgG, protein A and horseradish peroxidase (HRP)-conjugated goat anti-mouse Fc-specific IgG were from Sigma-Aldrich (St Louis, MO, USA). HRP-conjugated donkey anti-rabbit IgG was purchased from GE Healthcare and anti-β-tubulin mouse monoclonal IgG2b was from Millipore Corporation (Billerica, MA, USA). Block Ace (×20 concentrate of 2% [w/w] casein and 0.1% [w/w] Tween-20 in phosphate-buffered saline [PBS; 137 mM NaCl, 2.7 mM KCl, 10 mM Na_2PO_4, 2 mM KH_2PO_4, pH 7.4]) was purchased from DS Pharma Biomedical Co. Ltd. (Osaka, Japan). Biotinylated ZZ-BNC (1 μg mL^{-1}) and biotinylated protein A (1 μg mL^{-1}) were prepared with EZ-Link Sulfo-NHS (*N*-hydroxysuccinimide)-biotin (Pierce, Rockford, IL, USA) according to the manufacturer's protocol.

Sandwich ELISA

Capture IgGs (cIgG, anti-human desmin mouse monoclonal IgG2a [1 μg mL^{-1}]) in 15 mM sodium carbonate and 35 mM sodium bicarbonate buffer (pH 9.6) were adsorbed to each well (100 μL) of a Nunc-Immuno Plate II (96 wells; Nalge Nunc International K.K., Rochester, NY, USA) at 4 °C overnight, washed 3 times with 200 μL PBS containing 0.1% (v/v) Tween-20 (PBST), blocked with PBS containing 5% (w/v) Block Ace, and then kept at room temperature for 3 h. After washing with PBST 3 times, Ags (human desmin [0–32 μg mL^{-1}] in 100 μL PBS containing 5% Block Ace) were added to each well, incubated at room temperature for 1 h, and washed 3 times with PBST.

Detection IgGs (dIgGs, anti-human desmin mouse monoclonal IgG2a [1 μg mL^{-1}]) in 100 μL PBS containing 5% Block Ace were added to each well, incubated at room temperature for 30 min, and washed 3 times with PBST. Secondary antibody (HRP-conjugated goat anti-mouse Fc-specific IgG [0.1 μg mL^{-1}]) in 100 μL PBS containing 5% Block Ace was added to each well, incubated at room temperature for 30 min, and washed 3 times with PBST. When 0.1 μg mL^{-1} of biotinylated ZZ-BNC or biotinylated protein A in 100 μL PBS containing 5% Block Ace was used instead of the secondary antibody, the avidin–biotin complex (ABC) system (ABC peroxidase staining kit; Pierce) was used to detect biotin moieties in immunocomplexes with HRP. The HRP activity was determined with a 3,3′,5,5′-tetramethylbenzidine (TMB) substrate kit (Pierce). Absorbance at 450 nm was measured on a Varioskan microplate reader (Thermo Fisher Scientific, Waltham, MA, USA) using absorbance at 690 nm as the reference.

Sandwich immunoassay using QCM

Sandwich immunoassays were performed with a QCM model Twin-Q (As One Corp., Osaka, Japan). The sensor chip of QCM consisted of a 9 mm diameter disk made from an AT-cut 27 MHz quartz crystal with gold electrodes on both sides (diameter, 2.5 mm; area, 4.9 mm^2). A frequency change (ΔF) of 1 Hz corresponded to a weight change of 0.6 ng cm^{-2} (as calculated by the Sauerbrey equation).[19] The temperature of the measuring bath (500 μL) was maintained at 25 °C, with mixing at 600 rpm using a stirring tube. When a stable frequency (less than ±3 Hz) was observed for >1 min, the protein–protein interaction was judged to be equilibrated.

Before the immobilization of protein samples on the gold surface of the sensor chip, a piranha solution (1 : 3 H_2O_2 : H_2SO_4, 5 μL) was added to the gold surface at room temperature for 1 min to clean the surface, followed by thorough rinsing with distilled water. This procedure was repeated in triplicate. The gold surface was allowed to dry at room temperature before any frequency measurements were made. The sensor chip in the measuring bath was first treated with cIgGs (anti-human desmin mouse monoclonal IgG2a [2 μg mL^{-1}]), blocked with Block Ace (2 mg mL^{-1}), and then Ags (human desmin [0–4 μg mL^{-1}]) were added to the measuring bath. Detection IgGs (dIgGs, anti-human desmin mouse monoclonal IgG2a [2 μg mL^{-1}]) were added to the measuring bath, and finally, ZZ-BNC (2 μg protein mL^{-1}) was added. The measurements were repeated at least 3 times.

Atomic force microscopy

A bare gold substrate (1 × 1 cm; Auro sheet (111) HS; Tanaka Kikinzoku Kogyo K.K., Tokyo, Japan) was cleaned using 100 μL of piranha solution at room temperature for 1 min, rinsed with distilled water, and then dried at room temperature. Five microliters of protein sample (0.2 mg mL^{-1}) was spotted onto a gold substrate, incubated at room temperature for 30 min and washed with distilled water. When forming immunocomplexes, 5 μL of the next sample (0.2 mg mL^{-1}) in 0.2% Block Ace was spotted onto the same spot in a similar way. After drying in air, surface topographical images of the fabricated gold substrate were analyzed using an atomic force microscope (AFM) (model SPA-300; SII NanoTechnology Inc., Chiba, Japan). Raw AFM images were taken in non-contact mode in air at room temperature. The scanning rate was modulated for 1 Hz for a 500 × 500 nm scale image.

Fluorescence imaging

Anti-human desmin mouse monoclonal IgG2a (as cIgGs or dIgGs, 0.1 mg) and ZZ-BNCs (0.1 mg as protein) were labeled with Cy3- and Cy5-bis-reactive dyes (GE Healthcare) using NHS chemistry, respectively. Four types of gold substrates (diameter, 2.5 mm; area, 4.9 mm^2; the same as the QCM sensor chip) were prepared by spotting the following protein samples sequentially and at each step they were incubated at room temperature in the humidified atmosphere for 30 min: substrate A, 5 μL of Ag (0.2 mg mL^{-1}) followed by 0.2% Block Ace and 5 μL of Cy3-labeled dIgGs (0.2 mg mL^{-1}); substrate B, 5 μL of Cy3-labeled cIgGs (0.2 mg mL^{-1}) followed by 0.2% Block Ace; substrate C, 5 μL of cIgGs (0.2 mg mL^{-1}) followed by 0.2% Block Ace, 5 μL of Ag (0.2 mg mL^{-1}), and 5 μL of Cy3-labeled dIgGs (0.2 mg mL^{-1}); substrate D, 5 μL of Ag-Cy3-labeled dIgG complexes (0.4 mg mL^{-1}) followed by 0.2% Block Ace. Five microliters of Cy5-labeled ZZ-BNCs (0.2 mg mL^{-1}) were spotted onto each IgG spot on the four substrates and incubated at room temperature in the humidified atmosphere for 30 min. After washing three times with PBS, immunoreactive spots were visualized under a fluorescence image analyzer model OV-100 (Olympus, Tokyo, Japan). The fluorescence intensity of each spot (total 540 pixels) was quantitated using ImageJ 1.44o software (http://www.rsbweb.nih.gov/ij/).

Results and discussion

Effect of ZZ-BNCs on sandwich ELISA

Desmin is a 54 kDa subunit of 10 nm intermediate filaments;[20] therefore, anti-human desmin mouse monoclonal IgG2a can recognize multiple sites in intermediate filaments. We performed sandwich ELISAs for the detection of human desmin using the anti-human desmin mouse IgG2a as cIgG and dIgG simultaneously (Fig. 1B). When the immunocomplex of cIgG–Ag–dIgG was detected by HRP-conjugated goat anti-mouse Fc-specific IgG, the secondary antibody recognized both cIgGs and dIgGs simultaneously, and thereby a higher background A_{450} value was observed, independent of the amount of human desmin. When biotinylated protein A and the ABC system were used instead of the secondary antibody, the A_{450} value was increased marginally, according to the amount of human desmin. Weak detection of dIgGs, but not cIgGs, by protein A may be attributed to the size of protein A (see below). In contrast, the combination of biotinylated ZZ-BNCs (the structure of ZZ-BNC is described in Introduction and Fig. 1A) and ABC system showed a good response in terms of the A_{450} value to the amount of human desmin. Since biotinylated ZZ-BNCs could bind to both IgGs and avidin simultaneously,[14] it was suggested that ZZ-BNCs could detect dIgG efficiently and did not recognize cIgGs. When the mouse isotype control